2011

Planetary transit mapping of spotted stars with Kepler

Riley James Smith
Iowa State University

Planetary transit mapping of spotted stars with Kepler

by

Riley James Smith

A thesis submitted to the graduate faculty

in partial fulfillment of the requirements for the degree of

MASTER OF SCIENCE

Major: Astrophysics

Program of Study Committee:

Steven D. Kawaler, Major Professor

William Gutowski

Charles Kerton

Lee Anne Willson

Kerry Whisnant

Iowa State University

Ames, Iowa

2011

DEDICATION

I would like to dedicate this thesis to everyone who is bored with the ordinary.

TABLE OF CONTENTS

LIST OF TABLES

LIST OF FIGURES

ACKNOWLEDGEMENTS

I would like to take this opportunity to thank those who helped me with the various aspects of this project.

First and foremost, thanks to Steven D. Kawaler for his guidance throughout my research and the writing of this thesis. My graduate experience has been one I will never forget, and much of this is to your credit.

Thanks to the members of my committee for their input on the project, and the writing of this thesis.

Special thanks to Bert Pablo for his countless hours listening to my complaints about his model, and for never giving up. This thesis is made possible because of your hard work.

I also need to thank the *Kepler* team for prompt public release of the data on which this work is based, and for their outstanding efforts which have made these results possible. Funding for the *Kepler* mission is provided by NASA's Science Mission Directorate.

Finally, thanks to my family for their continued support in my endeavor as an astronomer. I'll see you all soon.

ABSTRACT

Stellar surfaces have been directly observed in primarily two limits of resolution. One provides a wealth of intricate observables and overwhelming detail in the case of our own Sun (Galilei 1613), equaled in measure by the difficulty to model such complex behavior. The other extreme provides scarce inferred detail (Gilliland & Dupree 1996) to simply none at all, for nearly every other star in the Universe. Transit mapping is a technique allowing for high-resolution analysis of surface inhomogeneities on active stars (those on the lower main sequence with convective envelopes) by using the system's planetary components as the surface probe. Observation from the ground is a daunting task. The necessary high precision photometry required to unambiguously identify and constrain stellar surface features is challenging because of atmospheric distortion and periodic coverage gaps due to Earth's rotation. To achieve the required precision for this technique to work effectively, it is necessary to take data from space, outside of the influence of Earth's atmosphere and rotation. The primary objective of the NASA *Kepler* Spacecraft is to search for planets via the transit method (Borucki et al. 2010), such that it's sensitivity towards the detection of these objects and it's capability to collect long stretches of uninterrupted coverage makes *Kepler* the idea instrument for analysis of time evolving surface features using transit mapping. In this thesis I use data taken by the *Kepler* spacecraft to model the spatial and temporal starspot coverage for HAT-P-11 (Kepler-3), a bright K4 dwarf in the *Kepler* field. The precision allowed by *Kepler* provides an opportunity to model stellar surfaces both in and out-of-transit, a unique ability unmatched by any other instrument or technique. In addition to having an activity map of the stellar surface, this study addresses correlations between stellar properties, starspot size and frequency, spot motion from rotation to rotation, and overall spot coverage.

CHAPTER 1. From sunspots to starspots

Ralph Waldo Emerson said, "The Sun shines and warms and lights us and we have no curiosity to know why this is so; but we ask the reason of all evil, of pain, and hunger, and mosquitos and silly people" (Emerson 1830). For centuries, humanity had taken this interpretation of the Sun, and more generally, all stars shining brightly in the night sky. Recognition and respect was given to the Sun as the defining source providing energy to the Earth, determining seasonal changes, crop cycles, and the primary basis for diurnal and annual timekeeping, but understanding of the Sun and the stars as complex and variable objects had to wait until both technology and society progressed to a level where such understanding could be treated on an objective basis.

Eventually it was accepted that our Sun was one of many stars in the Milky Way. It wasn't until Galileo Galilei first pointed his telescope at the heavens to recognize that the Sun was not the immutable object that classical Greek astronomers had postulated, but had imperfections and inhomogeneities on its surface, which were called sunspots. Centuries later, the most important insight into these strange spots came when George Hale discovered the magnetic nature of sunspots, where he observed the Zeeman splitting for several magnetically sensitive lines in the solar spectrum.

Modern astronomy has developed theories to explain the origin and evolution of sunspots. The next big step was to strengthen the solar-stellar connection with a general framework for starspots, built from theory but supported by observation. This thesis will attempt to contribute to the latter. Provided with the unmatched photometric data quality from the *Kepler* spacecraft, I will report on the temporal and spatial distribution of spots for one unique target observed by *Kepler*. The goal will be to provide a constrained map of the stellar surface using the novel technique of transit mapping in concert with high-precision photometry.

This chapter will address the overall motivation behind the project, with an overview of the origin and evolution of sunspots and starspots, as well as the observational techniques used to infer their structure, concluding with a discussion of what open questions can be addressed through this work. Chapter 2 will discuss the properties of the *Kepler* spacecraft, focusing primarily on the instrumental characteristics and how it applies to the project. Chapter 3 will describe the target system used for the focus of this project and the model developed to produce and also constrain the spot maps. Chapter 4 will present all data analysis and results, while Chapter 5 discusses the results of the analysis and provides a summary of the project.

1.1 How the star got its spots

The understanding of sunspots has progressed through a variety of interpretations as much as any bizarre astronomical phenomena. William Herschel, well known for his many contributions to astronomy, including the discovery of Uranus and his early model of the Milky Way, suggested that the Sun was a cool body surrounded by hot clouds. His inclusion of sunspots in this model were as holes in the hot clouds, revealing the cooler material beneath which he then postulated might be "richly stored with inhabitants" (Herschel 1795). Modern science has easily discounted such unusual ideas (Kawaler & Veverka 1981), but understanding the gamut of observed phenomena still remains a challenge.

1.1.1 Sunspots and the solar cycle - a touchstone for starspots and stellar cycles

As astronomers began interpreting sunspots as genuine physical phenomena on the surface of the Sun, many properties and behavioral patterns became apparent. Firstly, as resolution capabilities of telescopes increased, astronomers could easily observe the difference between umbral and penumbral regions in a spot. Figure 1.1 illustrates this general structure for sunspots.

This region appears dark with respect to the continuum of the photosphere due to the influence of magnetic fields. Without the presence of the magnetic field, gas pressure alone would provide the hydrostatic support of the gas against gravitational collapse. With the intrusion of magnetic flux through the photosphere, gravity is balanced by a combination of

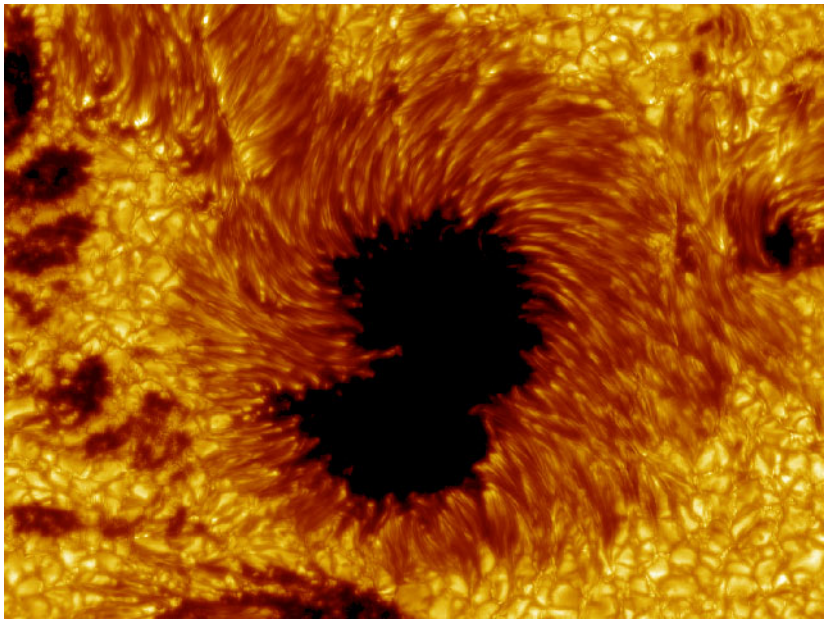

Figure 1.1 High-resolution image showing an active region with sunspots and pores. (Royal Swedish Academy of Sciences.)

gas pressure and magnetic pressure. This magnetic pressure reduces gas pressure by lowering temperature, and since the (local) flux is proportional to the local T^4, the emergent flux is lower.

The brightness of the umbra and penumbra in a spot differ due to the relative strength and orientation of the magnetic flux in each region, where the field is strongest and completely vertical with respect to the surface in the umbra, and weakest with a large inclination to the vertical in the penumbra. Typical flux values for solar umbra and penumbra are such that the umbra radiates only 20% of the photosphere continuum, resulting in a temperature difference of 2000 K, while the 'brighter' penumbra radiates 75% of the photosphere continuum, corresponding to temperature difference of 400 K (Thomas & Weiss 1992).

Sunspots are also observed in a variety of shapes and sizes. The theorist's dream is that of a non-rotating, circularly symmetric spot of constant flux, often without a defined penumbra (as we shall see in Chapter 3). But in reality, astronomers shall tire long before nature ceases to provide unpredictable and conceptually challenging phenomena, forever a step ahead. The largest sunspots have been observed to have diameters as large as 60,000 km, while the smallest

are on the order of 3,500 km (Thomas & Weiss 2008). Other magnetic inhomogeneities, called pores, are small-scale spots that have no penumbral region. Groups of many spots, pores, and faculae (introduced below) often appear together on the surface, which on such large scales are referred to more generally as active regions. The proximity of sunspots to one another will tend to distort any circular symmetry they might have had, and as they grow and decay, spots can coalesce with one another, dramatically altering their size and appearance.

The Sun displays brightening phenomena as well as the darker spots on the disk. Faculae and plages, bright patches located on the stellar surface, are also associated with magnetic activity and always accompany the formation of sunspots. Unlike spots, faculae and plages have a much lower contrast with respect to the photosphere continuum, with a temperature difference of about 100 K (Thomas & Weiss 2008). Bright spots on the Sun are the result of the 'missing' flux that is suppressed from the formation of cool spots. While these regions are important for determining the total irradiance of the Sun, for the purpose of this project they will be neglected because of the low contrast ratio, therefore smaller signal-to-noise ratio. These are also much more important for longer timescales (changing the overall continuum level of the entire star), whereas cool spots will have a large effect on short timescales.

Apart from variable morphology, sunspots also display variability in frequency (number) as well as in their observed location on the Sun (latitude). Spots appear to have an 11-year cycle from solar maximum to solar maximum; that is, we observe the largest coverage of active regions on the Sun every 11 years. At solar minimum, the Sun can show few to no spots, but as they increase in frequency at the beginning of the cycle, they do so breaking through the photosphere near 40°, then drifting equatorward as it reaches solar maximum. Large spots tend to form in pairs of opposite polarity, and the Sun shows an even longer period of 22 years where the polarity of each spot reverses. This means that the overall magnetic cycle of the Sun repeats every 22 years, where the sunspot cycle repeats every 11 years. This repeating pattern can best be shown with the so-called the butterfly diagram, first devised by Ernest Maunder in the early 20th century (Maunder 1904). Figure 1.2 displays the butterfly diagram atop a plot showing the average daily sunspot area from the late 19th century to recent years.

Obviously there must be a connection between this periodic behavior and the mechanism

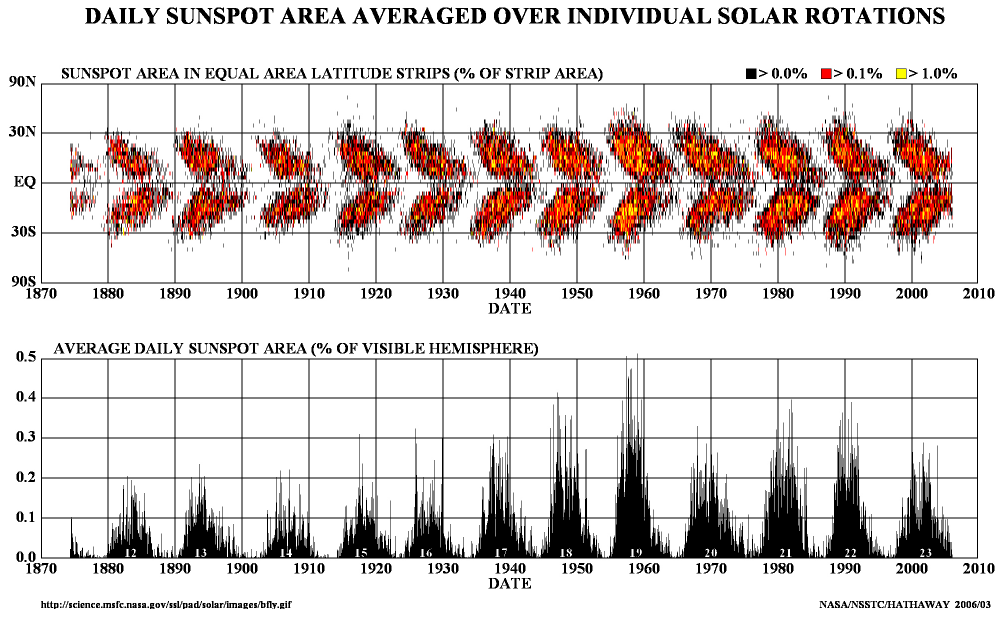

Figure 1.2 Sunspot cycles from 1878 to 2005. (NASA/NSSTC/Hathaway 2006/03)

driving the creation of sunspots. Thanks to the work of Thomas Cowling and Eugene Parker, this mechanism is best described through dynamo theory. In simplistic terms (!), dynamo theory is the theory that ascribes the continued existence of cosmic magnetic fields to induction effects in conducting fluid masses (Cowling 1981). A detailed explanation of dynamo theory is outside the scope of this project, but in the following section I will describe in what types of stars do we expect to see the consequences of such a theory in terms of observing magnetic inhomogeneities on stellar surfaces.

1.1.2 The solar-stellar connection

Thus far, the entire discussion has focused only on the Sun, and what we observe of its spot frequencies and distributions. Now we must make the connection between what we observe on the Sun, and what we expect to observe on other stars and why. The properties of the Sun as a star can be summarized in Table 1.1.

Table 1.1 Physical characteristics of the Sun. (Carroll & Ostlie 2007)

Spectral Type	G2 V
Age	4.57 Gyr
Mass	$M_\odot = 1.99\times10^{33}$ g
Radius (equatorial)	$R_\odot = 6.96\times10^{10}$ cm
Luminosity	$L_\odot = 3.847\times10^{33}$ erg s^{-1}
Effective Temperature	$T_{eff,\odot} = 5780$ K
Central Temperature	$T = 1.57\times10^{7}$ K
Central Pressure	$P = 2.34\times10^{16}$ N
log g	4.44
Rotation Period (equatorial)	25 days
Distance from Earth	1 AU = 1.496×10^{13} cm

The Vogt-Russel theorem states that given the basic stellar structure equations, constitutive relations, and boundary conditions, the mass and composition structure throughout a star uniquely determine its radius, luminosity, and internal structure, as well as its subsequent evolution (Carroll & Ostlie 2007). This theorem ignores the effects of magnetic fields, rotation, and other external factors (such as binary systems) that can affect a star's evolution, but in a simple manner this can help distinguish, specifically through mass, in what types of stars would we expect to see spots. The basic radial structure of the Sun ($M = 1\ M_\odot$) is shown below in Figure 1.3.

Here we see several distinct zones in the solar interior, namely the innermost radiative zone and the outer convective zone. The distinction between these two regions is determined by how energy is transported throughout the layers in the star. For stars of mass less than about 1.5 $M_\odot$, the proton-proton chain (Salpeter 1952) is the main energy source and radiation carries the energy outward toward the surface of the star until opacity, primarily due to neutral hydrogen, impedes the flow of ultraviolet photons and convection sets in. This convection zone increases with decreasing mass, where stars below $M = 0.3$ - $0.4\ M_\odot$ will be full convective throughout the entire interior (Mullen & MacDonald 2001). In stars more massive than about 1.5 $M_\odot$, the balance of gravity and pressure takes the central temperature in the CNO region (around 1.8×10^7 K) which has a much steeper temperature gradient than the pp-chain, enough so that radiation can no longer maintain the primary role of energy transport and convection

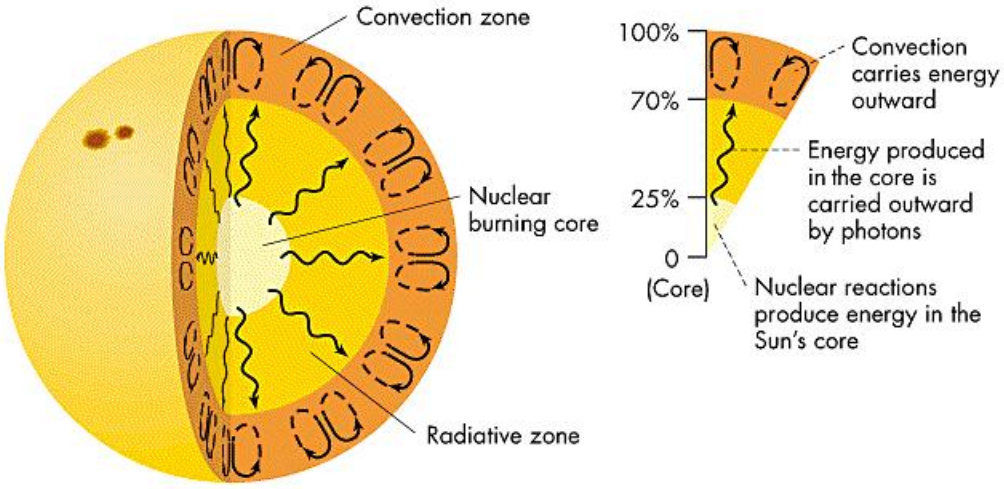

Figure 1.3 Schematic view of the interior structure of the Sun showing several distinctive regions. (www.physics.unc.edu/evans/pub)

sets in (Hansen et al 2004). It is in the former where conditions are met such that an efficient dynamo mechanism can be generated. In stars with convective envelopes, the intermediate layer separating the radiative region and the convective region, called the *tachocline*, is where the dynamo will act. The radiative zone rotates as a solid body, while the convective zone displays differential rotation and this discontinuity in Ω gives rise to shear forces, mixing material and generating a magnetic field which will eventually emerge through the photosphere as a starspot. As mentioned before, a full treatment of dynamo theory is outside scope of this thesis, as well as the complex physics describing the magnetohydrodynamic physics behind the production-to-emergence of magnetic flux bundles. As a first-order description, toroidal magnetic fields axisymmetric about the equator are generated as differential rotation drags out a preexisting azimuthally symmetric dipole field (Thomas & Weiss 2008). These toroidal fields are then subject to instabilities, creating buoyant forces, lifting the magnetic flux bundles through the

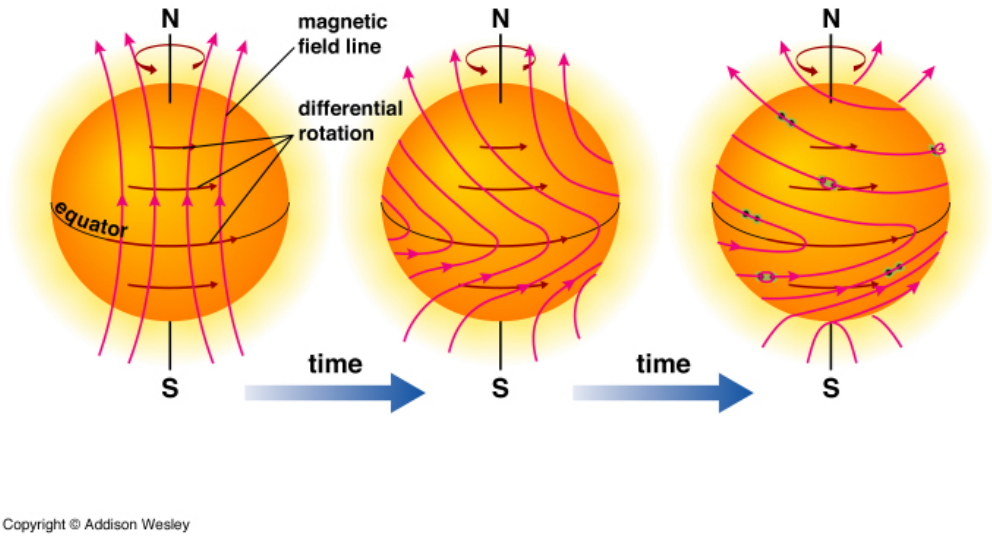

Figure 1.4 Diagram showing the differential rotation of the magnetic field. (Addison Wesley)

convective zone where they eventually emerge through the photosphere to form bipolar spots. In the Sun, this process repeats with a period of 22 years.

The rotation rate of a star and the depth of the convection zone in the envelope will be the primary factors determining the amount of magnetic activity. Rapid rotators, which for low-mass stars will imply younger stars due to rapid spin-down processes (Hansen et al 2004), will have higher amounts of activity than slow rotators (older low-mass stars). If stars which are fully convective or nearly so also rotate rapidly, there tends to be a saturation of activity because high levels of local angular momentum can in principle inhibit convection (large Reynolds numbers). This wraps up the brief discussion of theory behind the phenomena of starspots. The following section will review the variety of techniques used to detect the presence of starspots and their associated magnetic fields.

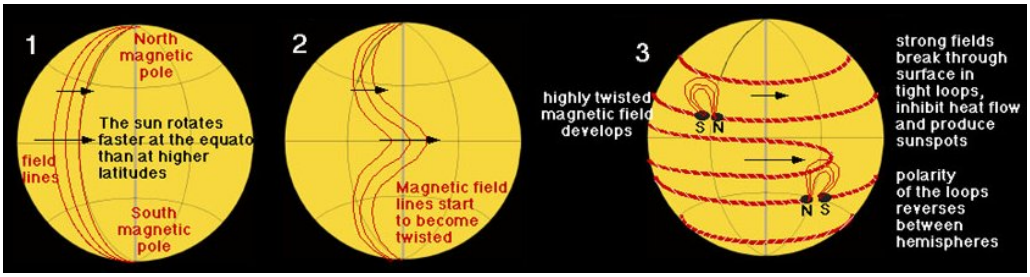

Figure 1.5 This diagram shows the emergence of magnetic flux through the photosphere. (www.land-of-kain.de/docs/spaceweather)

1.2 Observing techniques

Variable stars are a major focus in astrophysics, with the cutting edge currently being driven by the field of asteroseismology, the study of stellar interiors through their observed brightness changes. However, long before astronomers had detailed knowledge of stellar structure, stars observed with variable brightness patterns were assumed to have spots on their surface modulated by rotation, simply because that was what was observed on the Sun (Pickering 1880). We now know that most intrinsically variable stars are driven from pulsation mechanisms in the interior (opacity sources, turbulence, etc), but we also know that stars with convective envelopes can also show variable active regions across their surface. The challenge is how to to unambiguously derive the temporal and spatial spot evolution on these stars, as well as spot temperatures. If sufficient data are available, observations showing differential rotation and

stellar cycles analogous to the 22-year solar magnetic cycle would provide valuable information about the interiors of these stars.

1.2.1 Doppler imaging and Zeeman-Doppler imaging

For stars that have rotationally-broadened spectral lines, the technique of doppler imaging can determine a spot's size, shape, and position on the disc as well the stellar rotation period. As a spot traverses across the stellar disk, it causes a drop in the continuum emission, and this effect produces distinct deviations from the ideal rotationally-broadened absorption line profile. A simple model to explain this phenomena was first developed in the 1980s (Vogt & Penrod 1983), shown below in Figure 1.6.

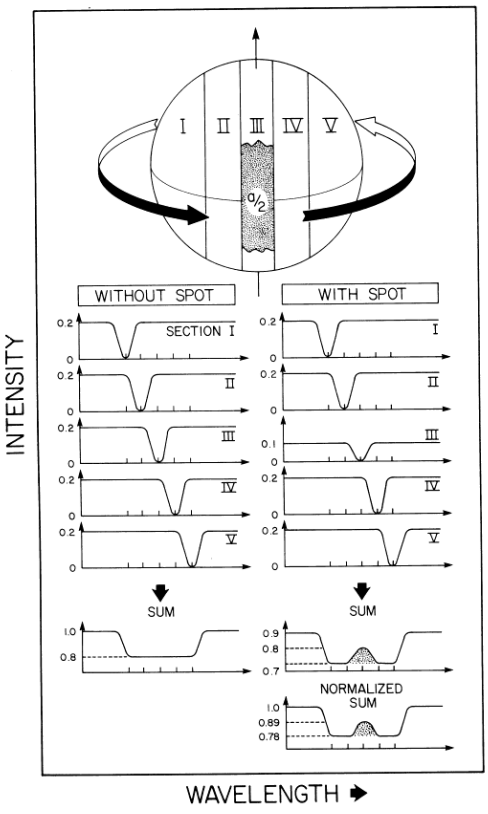

Figure 1.6 Illustration of the formation of apparent emission bumps in an absorption line of a rapidly rotating, spotted star.(Vogt & Penrod 1983)

Zeeman-Doppler imaging combines the technique of Doppler imaging with polarimetric measurements of spectral lines. One can detect stellar magnetic fields associated with spots

though the Zeeman signatures they generate in the shape and polarization state of spectral line profiles.

1.2.2 Photometry

Starspots can be observed with photometry as light-curve variations modulated on the rotation period of the star. Single color photometry provides the least amount of information compared to the other methods discussed here (with the exception discussed in the next section), as one cannot determine a unique solution to the spot sizes or configurations across the star. Forward models, as this project uses, attempt to reproduce the observed light-curve variability by creating models of spot distributions, often at fixed temperatures with idealized sizes and shapes. Two-color photometry can provide more information than single-color, thanks to calibrated dependencies of $T_{\rm eff}$ on color differences (Vogt 1981).

1.3 Goal of this work

This project will analyze data taken from the *Kepler* spacecraft to model the distribution of starspots in a unique system for which the transit mapping technique can derive unique results. Chapter 2 will describe the instrumental details of *Kepler*, how it can achieve unmatched photometric precision with its design, and specific instrumental peculiarities and how these affect the data from collection through reduction. But as described in the context of an observing technique used to derive information about starspots, *Kepler* is only a single-band CCD photometer, and this alone is shown to provide the least constraint of any method discussed above. The missing element is what makes the technique applied in this thesis so interesting: planet transits. The first transiting extrasolar planet was detected in 2002 (Charbonneau et al. 2000) by ground-based high-precision, high-cadence photometric measurements. Since this discovery, the theory describing and detection of extrasolar planets has blossomed into a major industry in astrophysics, thanks to the several instruments designed specifically for this task and to well-established observing techniques, much like those used to observe starspots and nonradial stellar pulsation.

Transiting extrasolar planets provide unique constraints on the analysis of starspots. As an extrasolar planet transits its host star, it partially blocks some of the star's light, and this signal (allowing for sufficient signal-to-noise) will show up as a characteristic U shape in the time series data. If an extrasolar planet transits across an active star, it can occult a spot and this will create a distinct bump within the transit signal itself. Because the geometry of the planet(s)

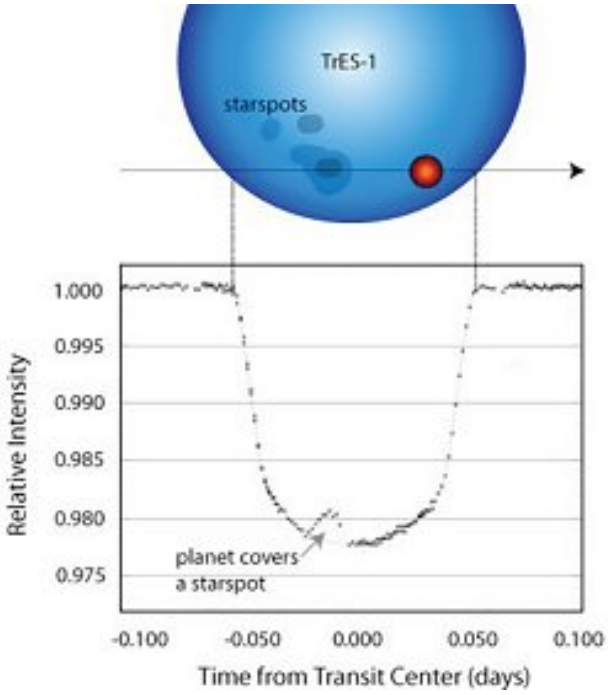

Figure 1.7 Schematic of a transit with spot (www.nightskyobserver.com/exoplanets)

and host star can be tightly constrained, the latitudes on the star at which the planet transits are well known, allowing the analysis method to break the otherwise degenerate distributions and sizes. Further constraint can be placed on the system if any planetary spin-orbit misalignment has been measure via the Rossiter-McLaughlin effect (Rossiter 1924; McLaughlin 1924). This effect is a measure quantifying how the orbital geometry of a transiting planet will dictate how it can alternately block blue-shifted or red-shifted (or both) light across the disk of a star. The goal of this work is to now utilize these unique methods and constraints as applied to the

fantastic precision of *Kepler* data. Accurate models of spot distributions, sizes, and temporal evolution patterns for stars of different spectral types, can provide insight into the complex interior structure and dynamo physics behind the generation and evolution of starspots. Better models describing the physics and consequences of starspots can then place further constraint on stellar evolutionary models, advancing our understanding of stellar astrophysics.

CHAPTER 2. *Kepler* - The right tool for the job

Modern time-series photometry is done predominantly with the aid of charge-coupled devices (CCDs). Specific detail about these detectors will be discussed further in Section 2.2., but the device can be generically described as a dense array of light-sensitive picture elements (pixels). The success of CCD application in astronomy is widespread, where the advantages a CCD provides over other light detectors has seen its implementation in astrometry, spectroscopy, photometry, as well as simple imaging.

Photometric time-series analysis in astronomy has two dominant criteria defining the performance of an instrument. The first is the photometric precision of the instrument itself. In broad strokes, this includes such factors as aperture size (how much light can you collect), pixel size, number & density, and whether your instrument is ground-based or space-based (atmospheric effects). The second dominant performance criterion is the temporal resolution of the instrument. The cadence at which data is collected and the duty cycle of observation can equally define how the data can be used (e.g. 30 min cadence data is adequate for characterizing most planetary orbits, but would give a poor representation of 5 minute solar-like oscillations).

The *Kepler* mission is an effort to maximize these performance capabilities, specifically with the goal of detecting and characterizing Earth-sized planets. The following is a general overview of the mission, instrumental design, and realized photometric performance of the *Kepler* spacecraft.

2.1 Mission Overview

The foremost goal of the *Kepler* mission is to determine the frequency and distribution of Earth-sized planets within the habitable zone of F - M main sequence stars (Borucki et al. 2010). *Kepler* utilizes the transit technique, continuously collecting photometry for ∼150,000 stars in the Cygnus region of the sky. The spacecraft is following an Earth-trailing 372.5-day orbit around the Sun with a mission life planned for at least 3.5 years, where in this timespan *Kepler* would be able to observe three transits of an Earth-Sun analog. Placing *Kepler* beyond Earth orbit avoids frustrations such as the South Atlantic Anomaly, atmospheric drag from the outer extent of Earth's atmosphere, Earthshine, and gravitational effects from Earth altering the orbit of the spacecraft. Along with the orbital period and relative size and distance of a planet to its host star that transit photometry provides, *Kepler* will provide a wealth of information on stellar activity and rotation periods.

2.1.1 Field of view

The optical axis of *Kepler* pointed towards RA = 19^h 22^m 40^s DEC = +44° 30' 00", ecliptic longitude and latitude of 307° and 65°, galactic longitude and latitude of 76.3° and 13.5°. The reason for choosing this position are manifold. The high ecliptic latitude points the spacecraft away from the Sun, where a simple sunshade blocks the light when the field of view (FOV) is in superior conjunction, allowing for continuous observation. The galactic latitude is high enough to avoid the large number of bright giants in the plane of the Milky Way, but low enough to still have a large sample population. The 1m class aperture opens to a FOV of diameter 16.1°, amounting to >100 square degrees of star field with which to collect data. Observing a single star field has several advantages over observing multiple fields over the lifetime of the mission. It optimizes the design of the spacecraft design, maximizes duty cycle, simplifies data accounting and processing, and generates long stretches of continuous data, an unprecedented volume of data available for asteroseismic analysis (Koch et al 2010). Figure 2.1 shows the *Kepler* FOV.

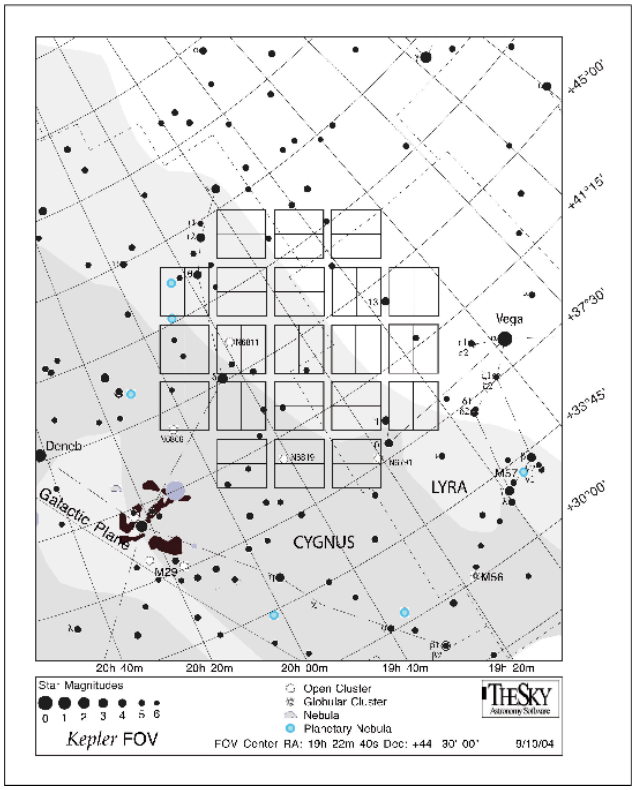

Figure 2.1 The Kepler field of view with CCD array overlaid. (KIH)

2.1.2 Searching for planets

Kepler's planet-detecting capabilities are primarily based on the Earth-Sun system. An Earth-Sun analogue will produce a signal of 84 parts per million (ppm) as per their ratio of areas, and a central transit length of 13 hours. The expected photometric precision for a 12^{th} magnitude G2V star is 20 ppm for a 6.5 hr transit, yielding a $\sim 4\sigma$ detection signal for an Earth-Sun analogue at half of the prototypical central transit time. Transits by terrestrial planets are expected to produce a change in stellar brightness from 50 ppm to 400 ppm lasting from 4 to 6 hours, where the geometric probability that a particular orbit is properly aligned to show transits is $\sim 0.5\%$ in or near the habitable zone (HZ) (Borucki et al. 2003).

Transit crossing events must be carefully characterized before they can be confirmed as bonafide planetary detections. The candidate system and the local neighborhood on the sky must be closely scrutinized to eliminate the possibility that a transit signal is being generated

by circumstances other than a planet occulting its host star.

To mitigate 'blend scenarios,' *Kepler* scientists have developed a characterization program including checks such as precise centroiding to show that the event was due to the target star and not an unresolved background event; high resolution ground-based and space-based (Hubble Space Telescope) follow-up photometry to resolve background objects possibly generating a transit-like signal; precise stellar radii determination derived from asteroseismological models, where a precise diameter for a star will increase the precision of the derived planetary diameter; characterization of intrinsic stellar variability using *Kepler* and ground-based data to properly assess contamination of the transit signal; and precise transit timing variation characterization to detect the influence of other bodies in the system.

Expected results are the discovery of giant inner planets with orbital periods of a few days within the first few months of the mission, objects with Mercury-like orbits detected within the first year. and the detection of Earth-sized planets within the full 3.5 year lifetime of the mission. Other expected results include the detection of non-transiting giant inner planets via their reflection profile on their host star, as well as systems with many planetary components.

2.1.3 Spacecraft & Photometer

The key to success with space-based time-series photometry is stability. To maximize the science capability of *Kepler*, this stability must be two-fold: the optics and electronics integrated into the detector array must be held within strict precision requirements as per the mission design, and the spacecraft itself must maintain a high level of pointing precision as it travels through space in its heliocentric orbit. Successfully extracting precision science from this instrument demands that each individual component within the system as a whole must be well characterized in terms of its intrinsic noise and how such noise manifests itself in the data, as well as any behavior that could be misinterpreted in the data as being of stellar origin rather than instrumental (periodic or not).

2.1.3.1 Telescope design

The *Kepler* telescope is a 0.95 m aperture wide-field Schmidt telescope. The orbit *Kepler* follows provides several key advantages for stable precision photometry. When compared to a low-Earth orbit, such as that followed by the CoRoT satellite (Auvergne et al. 2009), an Earth trailing orbit avoids phenomena such electronic interference when passing through radiation belts or the South Atlantic Anomaly, heating and cooling in and out of Earth's shadow, Earthshine, or drag induced by the thin exosphere of Earth's atmosphere. A schematic of the telescope components is shown in Figure 2.2.

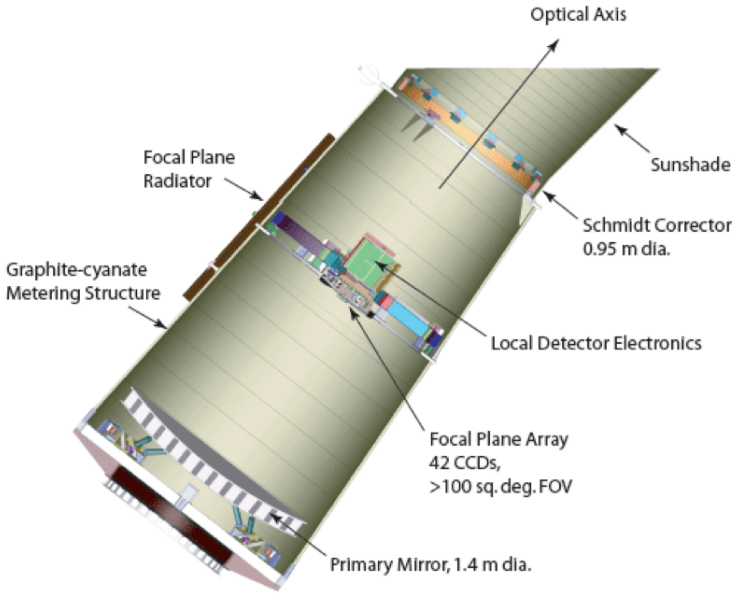

Figure 2.2 Schematic showing the instrumental design of the Kepler spacecraft. (KIH)

Not shown in Figure 2.2 are the additional elements making up the *Kepler* spacecraft, including the solar panels that protect the instrument and supply power, a sunshade that prevents light from the Sun from entering the detector when the target field is in conjunction with our star, a high-gain antenna with which *Kepler* transmits data back to Earth, a radiator to dump excess heat, and flight system elements to maintain spacecraft attitude.

2.1.3.2 Photometer spectral response

The spectral response of *Kepler* was designed again with solar-like stars as a focus. Light is collected in a "white light" band, slightly more broad than a combination of V and R bands. The upper and lower bandpasses between which the CCDs have $> 5\%$ response are 897 nm and 423 nm, respectively. The blue cutoff was chosen to avoid UV light. Although the majority of the solar irradiance variation comes from wavelengths < 400 nm, these photons only contribute 12% of the total solar flux (Koch et al 2010). The red cutoff was chosen to avoid fringing effects common in CCD photometry at red and infrared wavelengths. The net spectral response curve is shown in Figure 2.3.

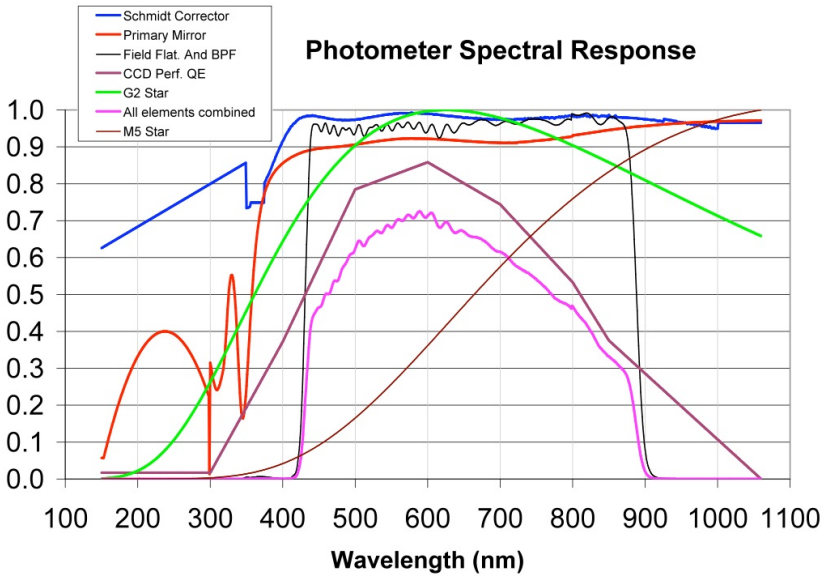

Figure 2.3 The combined spectral response of the Kepler telescope. (KIH)

2.1.4 Kinds of targets

Kepler collects data in two primary modes of operation. For long cadence (LC) targets, data is sampled every 29.4244 minutes and for short cadence (SC) targets, data is sampled every 58.85 seconds. Exoplanet candidates will be observed in both modes, where LC data is often used to identify signatures of transit events, then SC data can be used with its higher

sampling rate to improve transit timing, providing for more accurate solutions in characterizing planetary systems. In both LC and SC modes, individual frames with integration times set to 6.02 s with a readout time of 0.52 s are co-added to generate each science data point. The default number of frames for SC data is set at 9, nominally reading out data every minute, and 30 frames for LC data, reading out every ∼30 min. For transit mapping, SC data is most helpful because it samples at a rate high enough to resolve the small features present on the disk of a spotted star.

Other types of targets observed by *Kepler* are reference and background targets. Reference pixels are used to monitor the well-being of Kepler on a timeline more frequent than the monthly downlink. This data is downloaded every four days, and provides important information regarding the continued pointing precision of *Kepler*. Background targets, or background pixels, are used to characterize zodiacal light and the light coming from unresolved background stars. This data is collected at the LC frequency and downloaded monthly.

2.2 Detector Properties

2.2.1 Kepler CCDs

At the core of the photometer assembly is the 95 megapixel array of 42 science CCDs and four guidance CCDs. The CCDs are thinned, back-illuminated, dual output, 2200×1044 pixel devices. As discussed previously, a CCD is a two-dimensional array of in this case millions of photosensitive capacitors (pixels). Figure 2.4 show the focal plane of the 42 CCDs. The location on the sky of the optical axis was chosen as to minimize the number of bright stars on CCD, likewise to maximize the number of bright stars lying in gaps between the CCDs to avoid blooming, making precise photometry of neighboring stars difficult. There is a deliberate rotational symmetry designed into the layout of the 42 CCDs, such that charge bleeding due to bright stars on chip will contaminate the same portion of the sky with each quarterly rotation of the spacecraft.

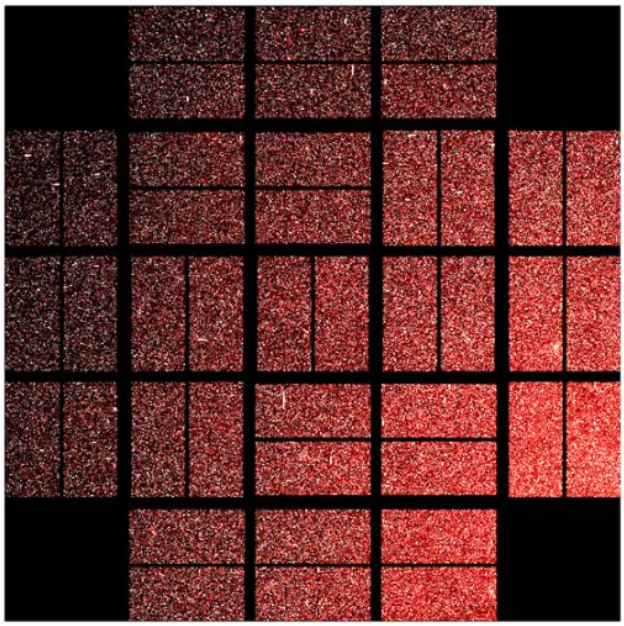

Figure 2.4 Kepler CCD alignment (http://astro.phys.au.dk/KASC/)

2.2.2 Noise

An Earth-Sun analog system will produce a transit lasting 13 hours with a signal of 84 ppm. For this signal to be detected with at $\geq 4\sigma$, the combined differential photometric precision (CDPP) must be $\leq$ 20 ppm. The CDPP is the effective white noise standard deviation over a specific time interval. The overall CDPP is a combination of several sources of noise, defined by (Koch et al 2010) as: CDPP = (shot noise^2 + measurement noise^2 + stellar variability^2)$^{1/2}$

Shot noise is a property common to all CCD detectors, where in samples of involving large numbers of photons, random fluctuations will occur in the collector because the number of photons arriving per second fluctuates. Measurement noise includes the detector and electronic noise (read noise), but also each other sources such as pointing jitter, stray light, sky noise and detector timing stability. The last and most difficult to noise source to characterize is the stellar variability as these tend not to be white noise processes. This is can be a particular difficulty for

stars with outer convection zones, where phenomena such as magnetic activity (spots, plages, flares etc), granulation, supergranulation and other convection driven variability can be a large contributor to the overall noise. Specific detail will be discussed below, but there have been many other very troublesome sources of noise discovered particular to the *Kepler* spacecraft. Most sources generating this 'extra' noise have been identified and can be accounted for in the data, other sources, or artifacts, yet remain a frustration, particularly in the frequency domain of data taken from *Kepler*.

2.2.3 Photometric Precision Estimation

The *Kepler Instrument Handbook* provides an estimate of the photometric precision attained with either LC or SC data for (isolated) K-F stars 12^{th} magnitude or fainter given by

$$P_0 = p\frac{\sqrt{f_{\rm Kep}t_{\rm int} + n_{\rm a}N_{\rm R}^2}}{\sqrt{n_{\rm fr}}f_{\rm Kep}t_{\rm int}}$$

and the photocurrent of each target in e-/s is $f_{\rm Kep} = 10^{-0.4(m_{\rm Kep}-12)}f_{\rm Kep12}$ Here $\rm f_{Kep12}$ is the photoelectron current for a 12^{th} magnitude star = 2.1×10^5 e-/s, $\rm t_{int}$ is the 6.02 second per-frame integration time, $\rm n_{fr}$ is the total number of frames in the benchmark 6.5 hour transit period, n_a is the number of pixels in the photometric aperture, $\rm m_{Kep}$ is the apparent *Kepler* magnitude, $\rm N_R$ is the read noise, and p is an empirical constant between 1 and 2 allowing for all other noise sources.

This expression does not include the effects of stellar variability, so a more accurate representation is given in the form similarly defined in the above section: $CDPP = \sqrt{P_0^2 + \sigma_{\rm ast}^2}$

2.2.4 Science CCD performance summary

Analysis of the first 43 days of data show that the lower bound of the photometric precision on transit timescales is consistent with expected shot noise levels. Gilliland et al. (2010) discuss specific details about the initial characteristics of *Kepler* SC data, where they show that the realized photometric performance in different brightness regimes reach levels approaching the fundamental limits imposed by Poisson statistics. Figure 2.5 taken from the *Kepler Data*

Characteristics Handbook plots the 6.5 hr temporal mean of the CDPP for first three-month stretch of data as a function of *Kepler* magnitude.

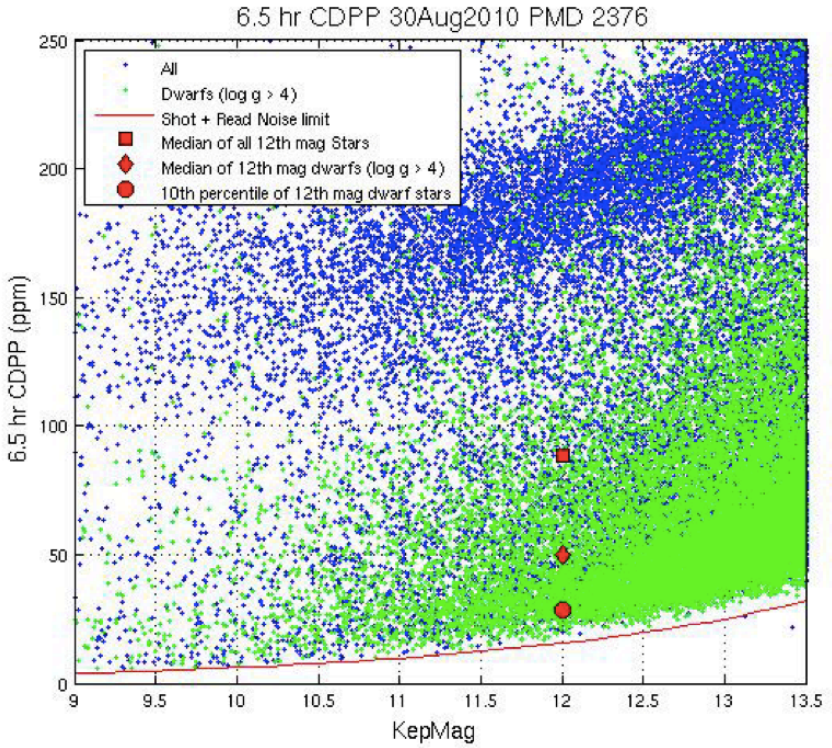

Figure 2.5 6.5 hr temporal mean of Quarter 2 CDPP time series for stars between 9th and 13.5th magnitude. (KDCH)

2.3 Instrumental perturbations & ongoing phenomena

As mentioned above, there are many systematic errors and instrumental perturbations in normal on-orbit operations of the *Kepler* spacecraft. These are caused by a variety of effects, including reaction wheel angular momentum desaturation, focus changes from heater fluctuation and outgassing, reaction wheel zero crossings, downlink Earth point where the spacecraft changes its attitude to point the high gain antenna at the Earth, *Agrabrightening* (an effect named for its discoverer where data point have an amplitude of many σ away from the average for an unknown reason), background time series, and pixel dropouts likely due to cosmic ray events.

Reaction wheels in the spacecraft counteract the torque from solar radiation pressure. When momentum levels in the wheels reach a saturation point (maximum operating RPM), they must dump the accrued momentum by firing thrusters every 3 days. The spacecraft loses fine point control over several SC cadences during these events, enough so that data affected by loss of fine point control is filtered out of data during initial processing. A second consequence of the same process, are data affected by the rumbling of the reaction wheel as it crosses zero angular momentum. This effect degrades the pointing on the timescale of several minutes, and increases the noise in the SC time-series data.

Safe mode events, where the spacecraft protects itself after some unanticipated response, have been the largest and most important interruptions in the history of *Kepler*. These interruptions can be on a time frame of several minutes to several days, and the data collected after resumption of science data show a tend related to the warm-up of the detector electronics.

For the purposes of this project, the most detrimental perturbation to the data are the safe mode events. The data used in this analysis are exclusively SC, where even with this cadence being the most affected by each different instrumental perturbation, the time scales over which the perturbations act are smaller than those on which the analysis is dependent (several hours - days), with the exception of safe mode events. One transit in the data set has suffered from loss of fine point control and had to be exempt from analysis, but safe mode events have lost two entire transits, where the lack of any information is much more detrimental than in a simple increase in noise.

2.3.1 Outliers, drifts & jumps

Defining outliers can be more an art than a science with *Kepler* data. The criteria based upon what level data can be safely removed is largely based on what outcome of the analysis is sought and what type of system is under analysis. For the asteroseismic study of solar-like oscillations in stars, outliers have been defined as individual measurements greater than 3σ away from the mean for SC data, and 5σ for LC data (Garćia et al. 2011). This choice of clipping standard removes approximately one percent of the data, primarily from loss of fine point control during momentum desats. For this project, very few outliers were clipped from

any data, due to the nature of the long time scales involved, and the rare incidence of an outlier affecting the analysis.

Drifts in the data are small low-frequency trends which in general are attributed to temperature changes in on board electronics, but can also be identified as long-term changes in pixel sensitivity. These can be corrected with functional fits to the thermal drift (Garćia et al. 2011), but caution must be used in the choice of reference, as in systems with high amplitude modulation in the local continuum from quarter to quarter.

Data jumps are similar to drifts as in they change the continuum level, but on a much shorter timescales. The mean value of a light curve can suddenly change due to attitude tweaks of the spacecraft or sudden pixel drops in sensitivity, among other reasons. During each downlink, *Kepler* shifts its position to point the high gain antenna at Earth, and this can lead to necessary attitude corrections to maintain the highest level of consistency throughout continued observation. Onboard software calculates the Maximum Attitude Residual, the largest distance between the expected and observed location of a star in its aperture for a given cadence, and performs corrections based on the criteria to minimize the RA, DEC, and roll errors to a value no larger than 100 millipixels (Garćia et al. 2011). Subsequent centroiding algorithm changes have been made to onboard systems to greatly reduce the boresight drift after the severity of the data jumps were first observed.

2.3.2 Light curves observed in more than one quarter

The mean flux level for a particular target can change drastically from quarter to quarter because after every quarterly roll in the orbit of *Kepler*, nearly every target is then observed on a different CCD with undoubtedly different characteristics than the previous. This is an issue in the data used in this project. To address this issue, we choose to use the first available quarter of data as reference, and normalized further quarters with respect to its mean level. For many stars, this correction can be both obvious and easy to remedy, but for systems which exhibit modulation in the overall light curves, this choice can have a significant impact on the results. The choice of 'maximum light' is important especially using the transit mapping technique, because the coverage of a spot or spots on the surface of a star is determined on the

relative change of light with respect to the local continuum of the photosphere.

CHAPTER 3. The system and the model

Discovery of the transiting extrasolar planet (TEP) HAT-P-11b (Bakos et al. 2010) was first reported by the HATNet project in early 2010. HATNet (Hungarian-made Automated Telescope Network) is a network of small-aperture, wide-field automated telescopes with the scientific goal of detecting and characterizing extrasolar planets. The project is based at two primary locations: the Fred Lawrence Whipple Observatory (FLWO) in Arizona and the Submillimeter Array (SMA) in Hawaii. At the time of its discovery, HAT-P-11b was the smallest radius TEP discovered from the ground, and the first "hot Neptune" discovered by transit searches.

This chapter will summarize the previously published results on this system and what makes it unique (and therefore difficult to model!), followed by a description of the code that I use to model this system.

3.1 The Star of the show - HAT-P-11

The star HAT-P-11 is host to the eleventh transiting system discovered by the HATNet team, a bright (V = 9.6), metal rich ([Fe/H] = $+0.31 \pm 0.05$) K4 dwarf star GSC 03561-02092 with the coordinates on the sky $\alpha = 19^h50^m50.21^s$, $\delta = +48^d04^m50.8^s$ (Bakos et al. 2010).

To correctly characterize a TEP, knowledge of the host star is important since the properties of the planet are relative to that of the host star. Table 3.1 summarizes the stellar parameters for HAT-P-11 from Bakos et al. (2010) (hereafter B10). The sources here are YY isochrones (Yi et al. 2001), "Spectroscopy Made Easy" (SME) (Valenti & Piskunov 1996), and *Hipparcos* distance data (Perryman et al. 1997).

To derive these parameters, B10 used a variety of assumptions and techniques. Initial values

Table 3.1 Stellar parameters for HAT-P-11

Parameter	Value	Source
$T_{\rm eff}$(K)	4780 ± 50	SME
[Fe/H]	+0.31 ± 0.05	SME
$v\sin i$ (km s^{-1}	1.5 ± 1.5	SME
M_* ($M_\odot$)	$0.81^{+0.02}_{-0.03}$	Y^2+Hip+SME
R_* ($R_\odot$)	0.75 ± 0.02	Y^2+Hip+SME
log g_* (cgs)	4.59 ± 0.03	Y^2+Hip+SME
L_* ($L_\odot$)	0.26 ± 0.02	Y^2+Hip+SME
M_V (mag)	6.57 ± 0.09	Y^2+Hip+SME
Age (Gyr)	$6.5^{+5.9}_{-4.1}$	Y^2+Hip+SME
Distance (pc)	38.0 ± 1.3	Y^2+Hip+SME

for the stellar atmospheric parameters were determined from spectra collected from the HIRES instrument on Keck I through the SME analysis package, yielding a surface gravity log g_* = 4.7 ± 0.1 (cgs), metallicity [Fe/H] = +0.32 ± 0.06 dex, effective temperature $T_{\rm eff}$ = 4850 ± 50 K, and a projected rotational velocity $v\sin i$ = 0.5 ± 0.5 km s^{-1}. From these values, B10 note that due to the indeterminacy for the assumed macro-turbulence for stars of this spectral type (K0 or later), they can only conclude that HAT-P-11 is a slow rotator, assigning it a projected rotational velocity $v\sin i$ = 1.5 ± 1.5 km s^{-1}. This value will be improved in the next chapter of the thesis.

To provide constraint on the luminosity of HAT-P-11, B10 use a combination of a reported *Hipparcos* distance of 36.4 ± 1.3 pc and apparent brightnesses in various photometric bands. The 2MASS K apparent magnitude K_{2MASS} = 7.009 ± 0.033 combined with the *Hippparcos* distance were used to derive an absolute magnitude of M_K = 4.18 ± 0.07. A Monte Carlo simulation was then run to search for best-fit stellar parameters. From the results of the simulation, B10 chose to keep the refined value of log g_* = 4.59 ± 0.03, and fix this value to repeat the SME analysis yielding $T_{\rm eff}$ = 4780 ± 50 K, [Fe/H] = +0.31 ± 0.05 and $v\sin i$ = 0.3 ± 0.5 km s^{-1}. Despite this result, the projected rotational velocity remained at the adopted values of $v\sin i$ = 1.5 ± 1.5 km s^{-1}. These results were adopted as the final atmospheric parameters for the star. A similar analysis was done for the stellar parameters, yielding $M_* = 0.809^{+0.020}_{-0.027}$ $M_\odot$, R_* = 0.752 ± 0.021 $R_\odot$, and L_* = 0.26 ± 0.02 $L_\odot$.

A key observation noted in the analysis of B10, is the periodic modulation of the light curve. Detected in both an autocorrelation function and in a Fourier power spectrum, they recovered a period of $\approx$ 29.2 days. This result was easily interpreted as a variation in light due to the presence of spots carried across the stellar disc by rotation. Assuming this as the rotation period for HAT-P-11, that implies an equatorial velocity of $v_{eq} = 1.3$ km s^{-1}, which is consistent with the previously adopted range.

3.1.1 *Kepler* observations of HAT-P-11

The analysis presented in this thesis will be largely based on the results of B10, and in several cases will allow for improvement thanks to the outstanding data quality from *Kepler*. Below is the *Kepler* light curve for HAT-P-11 (also known as Kepler-3) from the first ~140 days of the mission. Several gaps are visible from safe mode events in the spacecraft (at ~54962,

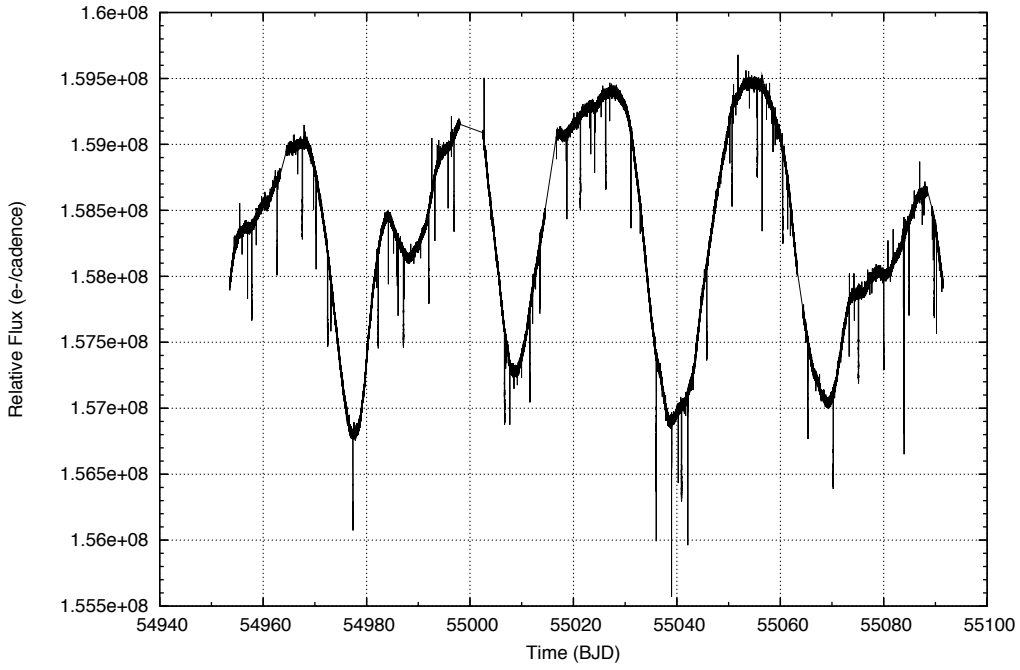

Figure 3.1 *Kepler* light curve for HAT-P-11

55000 and 55065 days, etc.). The latter two-thirds of the data have been corrected for a DC-

level continuum brightness difference (due to an attitude change in *Kepler* after downlink). The overall modulation of the light curve shows a ∼1.6% change in brightness with a period of about 30 days, in close agreement with the HATNet observations. To better determine the period of modulation (assumed to be the rotation period of the star), the *Kepler* data were subject to a Fourier spectrum analysis and a phase dispersion minimum analysis. The results from the Fourier transform shows a dominant peak a period P_{rot} = 30.65533 days, while the phase dispersion minimum is for a period P_{rot} = 30.54907 days. The adopted rotation period used throughout further analysis is chosen as P_{rot} = 30.65533 ± 6.63×10^{-4} days.

Also visible in the light curve for HAT-P-11 are the transits of HAT-P-11b, as well as many bad points, mimicking the drop in light due to a transit. These points can occur when *Kepler* temporarily loses fine point control or focus for several SC integrations (as most of these only last for ∼3-4 successive points).

3.2 HAT-P-11b: a hot Neptune with an unusual orbit

At the time of discovery, HAT-P-11b was the smallest radius TEP discovered from the ground, and the first "hot Neptune" discovered by transit searches. The properties of HAT-P-11b as measured by B10 are as follows: R_p = 0.422 ± 0.014 R_J (4.73 ± 0.16 $R_\oplus$), M_p = 0.081 ± 0.009 M_J (25.8 ± 2.9 $M_\oplus$), a = $0.0530^{+0.0002}_{-0.0008}$ AU, e = 0.198 ± 0.046, ω = 355.2° ± 17.3°, and P = 4.887816 ± 0.0000071 days. For comparison, Neptune has a mass and radius of 17 $M_\oplus$ and 3.8 $R_\oplus$ respectively and follows a 165-year orbit with a semi-major axis of 30 AU, producing a transit length of 71 hours at a depth of 0.127%. Figure 3.2 gives an up-close look at one (unspotted, phased, normalized) transit by HAT-P-11b.

The orbital period of HAT-P-11b was improved using a simple linear interpolation T = T_0 + P×E, where E is the epoch of the orbit, T_0 is the intercept and P is the period. Fitting the time of minima for all transits to this expression yields a new period P = 4.887804 ± 2.311×10^{-6}. This period is adopted through the rest of the analysis to follow.

HAT-P-11b is interesting for several reasons. Firstly, using planetary isochrones from Baraffe et al. (2008), B10 conclude that the best match for the observed properties of HAT-P-11b appear to be a super-Neptune with Z = 0.9 (heavy elements) and a 10% H/He envelope. The

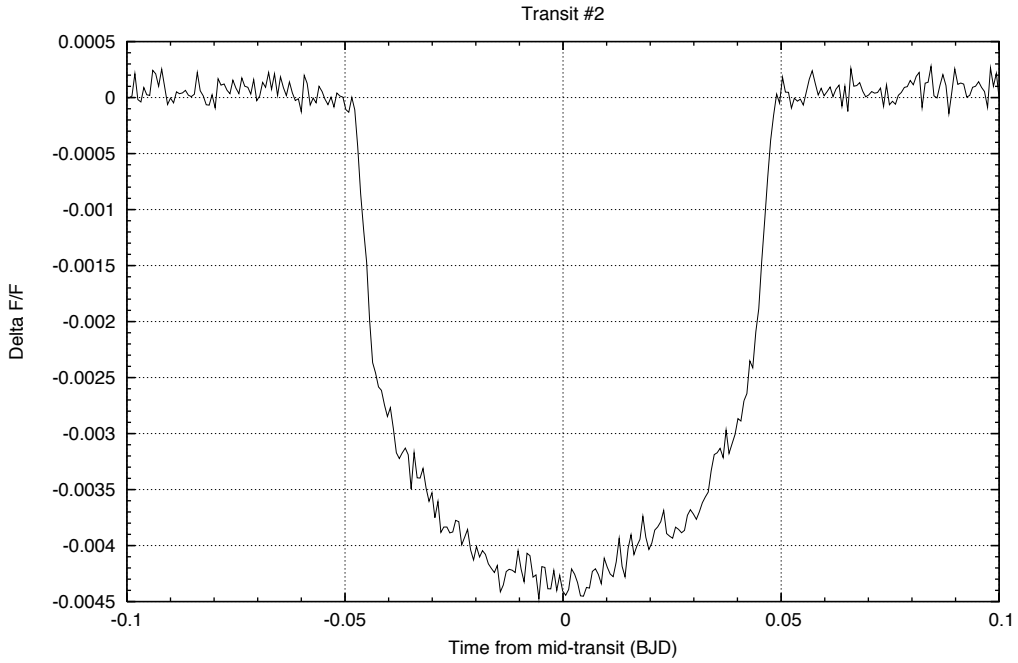

Figure 3.2 Unspotted transit example

models used to determine these parameters describe an extremely metal-rich, non-irradiated planet aged somewhere between 3-7 Gyr old.

Equally interesting, and unexpectedly beneficial for the purpose of this project, HAT-P-11b follows an eccentric orbit ($e = 0.198 \pm 0.046$) at an extreme spin-orbit misalignment ($\lambda = 103^{+26}_{-10}$ deg) (Winn et al. 2010). The oblique orbit has measured through the Rossiter-McLaughlin effect (McLaughlin 1924; Rossiter 1924), wherein during a planetary transit, the planet preferentially blocks some red-shifted or blue-shifted light (due to the rotation of the star towards and away from the light-on-sight) based on the geometry of the orbit. This angle λ represents the difference between the axis of rotation of the host star, and the axis about which the planet orbits. A system where $\lambda = 90°$ would represent a planet on a polar orbit around its star. Figure 3.3 shows a schematic of the transit path across the surface of the star.

An unusual orbit such as this is likely the result of a scattering event with another planet

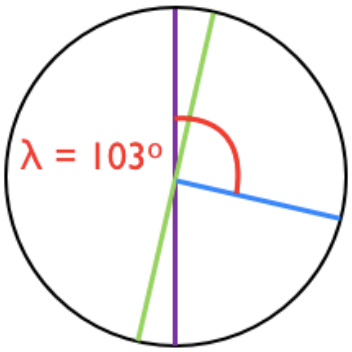

Figure 3.3 Sketch of planet transit path. The purple line represents the stellar rotation axis, and the green line $\sim 13°$ away from the stellar rotation axis represents the path of the planet. Perpendicular to this path, the blue represents the planetary orbital axis.

early in the history of the system. This is very advantageous for applying the technique of transit mapping, because now our "probe" transits at all latitudes of the stellar surface, completely sampling the whole of the star for evidence of spot activity. Combined with the information provided from the out-of-transit light curve, this unique alignment allows for a very precise determination of spot radii, latitudes, and longitudes.

3.3 The model

In order to generate a surface spot map, a model had to be developed that could recreate this rich system, specifically from the eyes of *Kepler*. Thanks to the hard work of Iowa State graduate student Bert Pablo, a code was developed to be used to accurately simulate *Kepler*

light curves of spotted stars undergoing planetary transits. The code is able to reproduce the cadence (SC) and noise characteristics of the *Kepler* spacecraft, the expected limb-darkened brightness of a given star as observed by *Kepler*, the geometry, transit depth and timing of a planetary companion, and the presence of spots carried across the surface of the star by rotation.

3.3.1 Input parameters

3.3.1.1 The star

The star in the model is described by inputting the B and V magnitudes, the stellar mass and radius, the rotation period, limb darkening coefficients, and the inclination angle. The B and V magnitudes are used to determine the *Kepler* magnitude, as well as the total flux. HAT-P-11 has B = 10.66 ± 0.05 and V = 9.473 ± 0.023 (Hog et al. 2000). The stellar mass is used to refine the orbital properties of the planet, specifically the known velocity differential during transits due to eccentric orbit and large argument of periastron (transits occur ∼5° prior to periastron). Limb darkening coefficients and the stellar radius are necessary to correctly reproduce the planet transit depth and shape, for a given planet size. The limb darkening law used in the model is quadratic in form such that $\frac{I(\mu)}{I(1)}$ = 1- a_1(1-μ) - a_2(1-μ)^2 with a_1 = 0.8771 and a_2 = -0.0299 (Claret 2004). These coefficients were chosen from a grid of models, where the parameters defining the stellar model match most closely those of HAT-P-11 (log g_* = 4.5, T_{eff*} = 4750 K, [Fe/H] = +0.3) and the bandpass for which they are calculated best matches the *Kepler* bandpass (in this case Sloan g'). The stellar radius in combination with the planetary radius defines the transit depth, so here value is adopted from B10 as R = 0.752 $R_\odot$.

The stellar rotation period and inclination angle are crucial elements to this project. The rotation period was quoted earlier as P_{rot} = 30.65533 days. This is assumes solid-body rotation for the star, which is counter to most low mass stars (stars with convective envelopes), but this effect will be identified in the data and addressed in the following chapter. Lastly, the inclination angle is very important as it determines what longitudes and latitudes are observable on the

star at any one time. This is the reference for which the spherical coordinates on the surface of the star are derived from. From the large transit depth, one can assume that the stellar inclination angle must be $\sim 90^\circ$ (where 0° would be pole-on), but for a planet with such an odd orbit (nearly polar!), the inclination of the host star cannot be treated arbitrarily. Having said that, the lion's share of the modeling was done using an arbitrary inclination angle $i = 88.5^\circ$. As shown in the next chapter (modulo some reasonable assumptions), fixing this angle allowed us to measure the actual inclination of the stellar rotation axis, which is *not* the assumed value.

3.3.1.2 The planet

Defining the planet in the model was much simpler than the star. The planet does not radiate in the model, so it does not require any color or temperature information. This does not reflect reality, but for the purposes of this project, it is used simply as a probe for starspots, not as the object of study itself. The most important parameter describing the planet is the radius. B10 find the radius of HAT-P-11b as $R_p = 0.422 \pm 0.014$ R_J. In theory, with a limb-darkened star, and a correct ratio of areas ($\frac{R_p^2}{R_*^2}$), there is no reason why the model used for this project should not be able to reproduce the observed transit depth $\frac{\Delta F}{F} = 0.439\%$. However, this is not what is observed. Using the published values for R_p and R_* derived from B10, the observed transit depth is underestimated as $\frac{\Delta F}{F} = 0.328\%$. The observed transit depth is closer to the expected depth of a stellar disk of constant brightness (no limb-darkening) using the quoted radii for this system ($\frac{\Delta F}{F} = 0.318\%$). To account for this difference and to reproduce the observed transit depth, the planet radius had to be artificially inflated such that $R_p = 0.498$ R_J, assuming the radius of the star is fixed at the B10 value. The transit depth could have been increased by artificially making the star smaller than the published value, but this was dismissed as there are other methods to constrain the radius of the star that are independent of the size of the planet, but not vice versa. Adding to the conundrum, the expected transit depth for a star of constant brightness using the B10 stellar radius and the new 'inflated' planetary radius yields $\frac{\Delta F}{F} = 0.442\%$, which is close to the observed transit depth, but not an exact match. This line of reasoning tends to indicate that the overall brightness of the limb-darkened star is not being treated correctly in the model, even when model simulations of transit ingress and egress

show quite clearly that limb-darkening is included. The possibility that B10 have incorrectly interpreted their results cannot be completely dismissed, but considering the evidence discussed here, this is a very unlikely origin for the discrepancy.

Inflating the planet to match the observed transit depth also changes the length of the transit (for the same chord). To account for this, the transit velocity gradient

$$\left[v_\theta = \frac{2\pi a(1+\sin\theta)}{\tau(1-e^2)}, v_r = \frac{2\pi a e \sin\theta}{\tau(1-e^2)}\right]$$

was scaled up, such that the time in transit with the larger planet was equal to that of the smaller planet (make the larger planet move faster). This maintains the in-transit timing consistency, which is very important when deriving starspot radii.

The orbital period, as derived from linear interpolation of times of minima, is input as P = 4.887804 ± 2.311×10^{-6} days and the initial timing of the first transit (when does the planet reach first contact in the first transit) is also an input parameter. The last parameter to describe the planet is the spin-orbit alignment angle described above, and for HAT-P-11b this angle is reported as $\lambda = 103^{+26}_{-10}$ deg.

3.3.1.3 The spots

To fully characterize spots, we would requie approximately 7 separate parameters. In this study we vary 4 of them: percent flux drop, radius, latitude and longitude. Other parameters that could be used to describe the evolution spots are start time (when is the spot first observed?), growth time (how long does it take for a spot to fully develop?), and decay time (how long does the spot live?). The percent flux drop inside a spot has been fixed for this project, derived from a spot temperature contrast defined by Berdyugina (2005). This work plots the spot temperature contrast with respect to the photospheric temperature in many active giants and dwarfs. From this plot, the spot temperature contrast for a star with photospheric temperature of T_{eff} = 4780 K can be estimated as T_{phot} - T_{spot} ≈ 1150 K. This implies a spot temperature T_{spot} ≈ 3630 K, and thus transfers into a flux ratio $\frac{T_{spot}}{T_{phot}} = 0.3326$ or a relative flux drop of ∼67% of a spot with respect to the photosphere. All spots in this project are assumed to be perfectly circular with no penumbra, moat, etc. for the sake of simplicity. There is strong

evidence for "active regions" in the data (areas with no leading spot, but observable levels of magnetic activity), but this cannot be accurately modeled as these regions tend to consist of many individual inhomogeneities (both dark and bright). There is also some evidence towards the presence of large penumbra regions surrounding the darker spots, but again for simplicity, these were not included into the model parameters.

The spot radii, longitudes and latitudes were the real workhorses of this project. These are the three parameters than were varied during each iteration of the model. Figure 3.4 shows an example of a phased, normalized transit that occults a starspot on HAT-P-11. From the

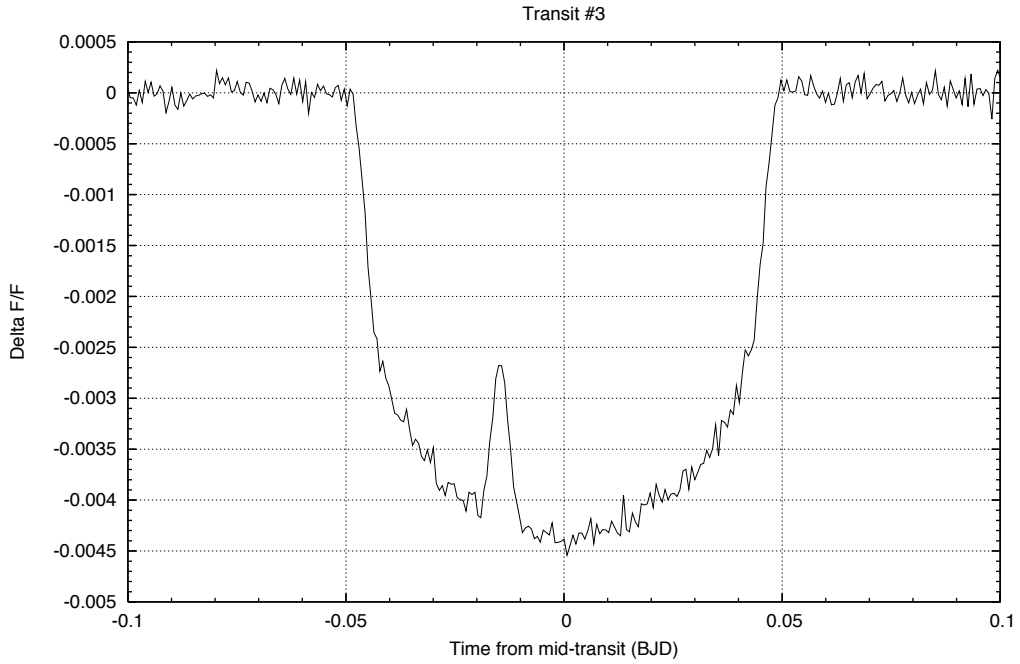

Figure 3.4 Spotted transit example

known geometry of the orbit of HAT-P-11b, the latitude and longitude of the spot can be well determined. More detail on this process is given in the following chapter.

CHAPTER 4. Analysis & results - stellar geography

4.1 Methodology

The goal of the analysis is to determine the size, latitude, longitude, and frequency of spots on the surface of HAT-P-11. We employ a variety of techniques (see discussion in Chapter 1), but the advantage of using transit mapping is the level of degeneracy that can be lifted towards an unambiguous solution. Prior knowledge of the system geometry, combined with information from both in and out-of-transit light allows us to distinguish between degenerate solutions in spot locations, specifically their longitude. Below begins a discussion of the most evolved methodology used for this work.

4.1.1 Modeling spots in-transit

The primary focus of the modeling effort was in determining spot parameters individually on a per-transit basis. Each transit was inspected for the characteristic 're-brightening' signature of the transiting planet occulting a spot. Where in most cases this signature was unambiguous, to assist in identifying spots, we built an empirical template of averaged, unspotted transits. This template also provides an estimate of the characteristic noise level for 'quiet' transits across HAT-P-11. A simple calculation of the standard deviation $\sigma = \sqrt{\frac{\Sigma(x-\bar{x})^2}{N-1}}$ of these residuals show that for an average unspotted transit (not including data outside of the transit), the noise level in the data is $\sim$70 ppm. This estimate is supported from results of repeating this process with spotted transits, where as expected the noise levels rise significantly (indicating non-gaussian behavior), easily ranging from $\sim$100 ppm to $\sim$300 ppm. Figures 4.1 and 4.2 show an example of a spotted transit before and after applying our template.

These figures are limited in phase to first and last contact of the transit. The departure from

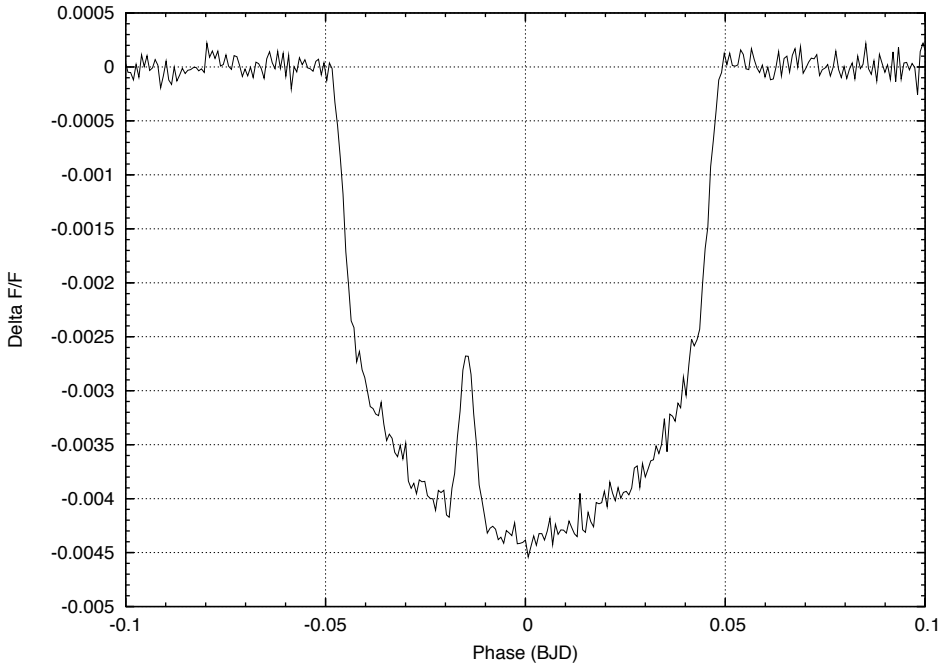

Figure 4.1 Example of a spotted transit before applying the unspotted template.

the mean during ingress and egress (the first and last moments of the transit) are due to an incomplete treatment of limb-darkening in the version of the code used to produce these plots. For the purposes of this project, measuring the signal strength of spots in this manner was used primarily as a phenomenological criterion, to help visually distinguish between what might be occultation events of individuals spots or transits across more ambiguous active regions, and to provide a base-level estimate of the typical noise in a transit. Figure 4.3 shows a transit with no distinctive spot occultation overlaid with a transit containing three unambiguous spot signals.

The transit path of HAT-P-11b was known very well, so estimating a latitude of a spot was easy to determine as the time of a spot brightening gives the latitude of the spot. Calculating the spot longitude as a function of time was likewise trivial to compute (assuming the stellar rotation period derived in Chapter 3). With the position determined in this way, the duration of the spot transit and its height combine to help determine the size of the spot. The process

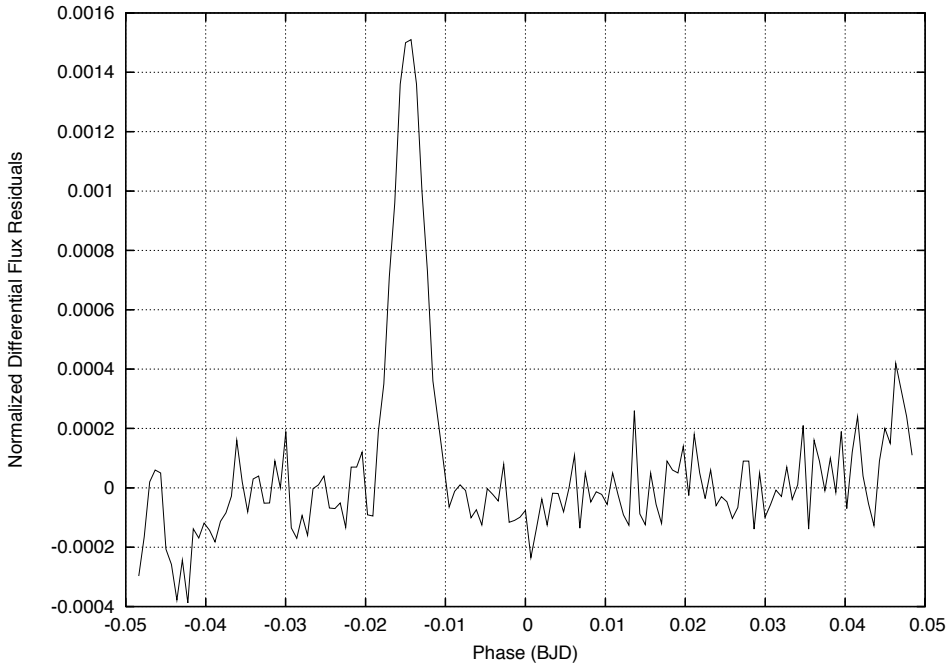

Figure 4.2 Example transit residuals of a spotted transit normalized to the unspotted template.

of refining these measures to find a realistic solution required an iterative process.

This process was repeated until a set of given parameters could accurately enough reproduce the light curve in an observed transit. An example of model output overlaid atop observed data is shown below. The results from repeating this process for each transit are shown in Table 4.1

Transits in which more than one spot are occulted are grouped together with the designations a, b, c. All quoted errors are defined as the minimum change in any one variable to generate a signal difference of 100 ppm, a value taken as the average error estimate at any one place in the light curve. The uncertainty in radius is calculated using $\Delta \mathrm{R_{spot}} = \mathrm{R_*}\sqrt{\frac{1-(1-\frac{\Delta F}{F})(1-\frac{R^2_{\mathrm{spot}}}{R^2_*}\times 0.358)}{0.358}}$-$\mathrm{R_{spot}}$ where 0.358 is the flux of the spot relative to the photosphere, and the uncertainty in latitude and longitude are calculated using $\Delta\mathrm{Lat} = \frac{\Delta R_{\mathrm{spot}}}{R_*}\times 180$ and $\Delta\mathrm{Long} = \frac{\Delta b_{\mathrm{spot}}}{R_*}\times 180$, where b is the semi-minor axis of the projected spot area.

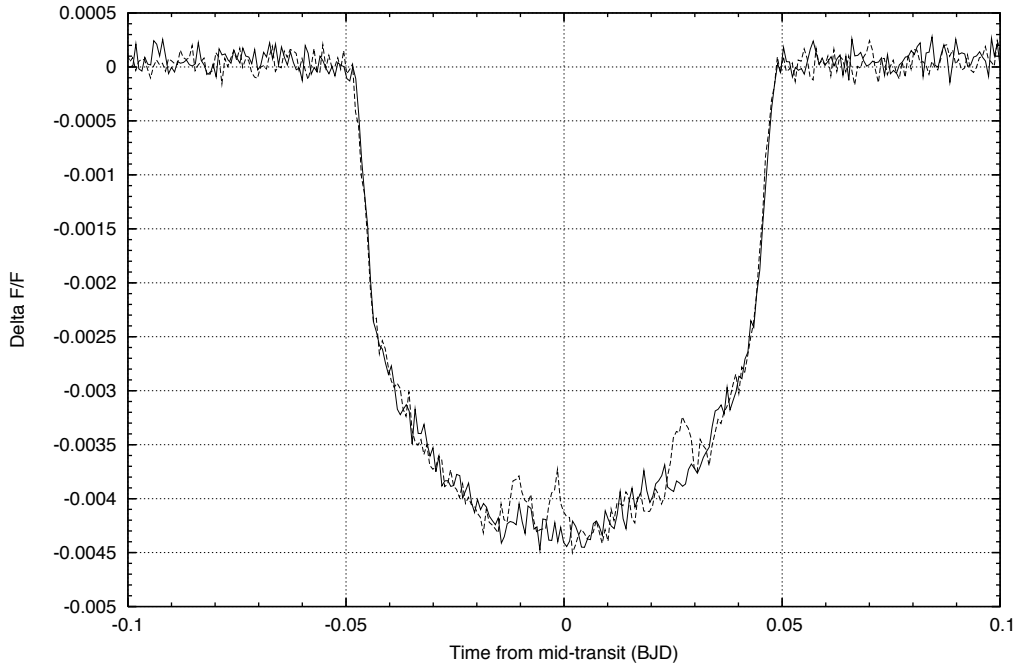

Figure 4.3 Multiple spots in transit - The solid line is an unspotted transit, while the dashed line show a transit with three distinct spots in the transit path.

Several samples were tested to find the characteristic error floor of 100 ppm, and each sample was selected in the quietest regions in the light curve (flattest, outside of the influence of any instrumental disturbance). Such a selection criterion can gauge this error measurement as a lower limit on the noise for this target. It is important to note that this list does not comprise a final or necessarily complete tally of independent starspots. Spots listed in Table 4.1 are solutions treating each transit as independent from one another, and only for spots that had a significant signal-to-noise ratio $\gtrsim 3\sigma$ in transit. This list does not consider recurring spots in the simulation (e.g. spot-in-transit 1 observed in transit 20), it assumes solid-body rotation on the surface of the star (no differential rotation with latitude), spots are all of a constant flux ratio with respect to the photosphere, have no fine structure (umbra only), and all spots are permanent (no spot growth/decay). The choice of stellar inclination is also very important, as the definition of i will also define the frame of reference for which the latitudes

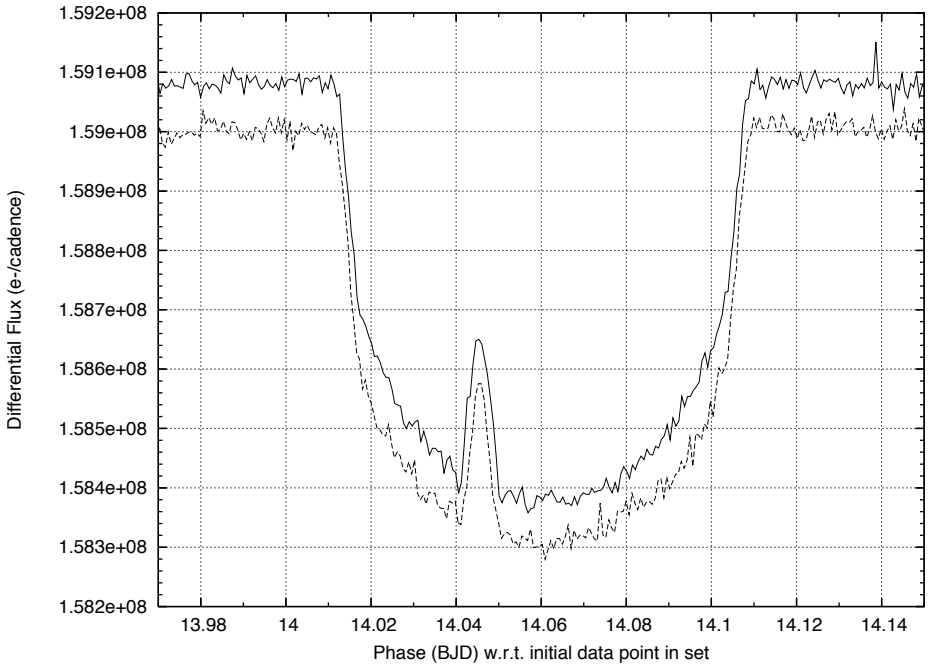

Figure 4.4 Comparing model output with data - the solid line indicates model output and the dashed line is the actual data (arbitrarily offset).

of each spot is determined.

4.1.2 Using out-of-transit light

The spot parameters derived from the in-transit light have little degeneracy in terms of the size of the spot (assuming a fixed contrast ratio, shape and structure), no degeneracy in latitude (assuming the geometry from the Rossiter-McLaughlin measurements are correct), but two-fold degeneracy in longitude. That is to say, if during a transit, the planet has a grazing path along a chord rather than a diameter, there is no definitive way to say if the grazing eclipse happened with respect to the leading or trailing edge of the spot using the in-transit information. To lift the degeneracy, the out-of-transit light must be considered. Observing the shape of the light curve as a whole can identify the relative phase difference between minima in the data and the minima imposed by placing individual spot solutions in the model. Although

this is not a quantitative solution for breaking the degeneracy, in almost every individual transit solution, the relative phase of local minima and imposed minima was unambiguous and it was then clear whether a grazing spot occultation was either leading or trailing. Transit #24 shown in the Figure 4.5 is one of the more clear examples of this effect. The local minimum is located 'behind' the transit in time, which identifies the spot observed in transit #24 as being an leading-edge occultation (assuming the spot observed in this transit contributes to the local continuum depression, which it must).

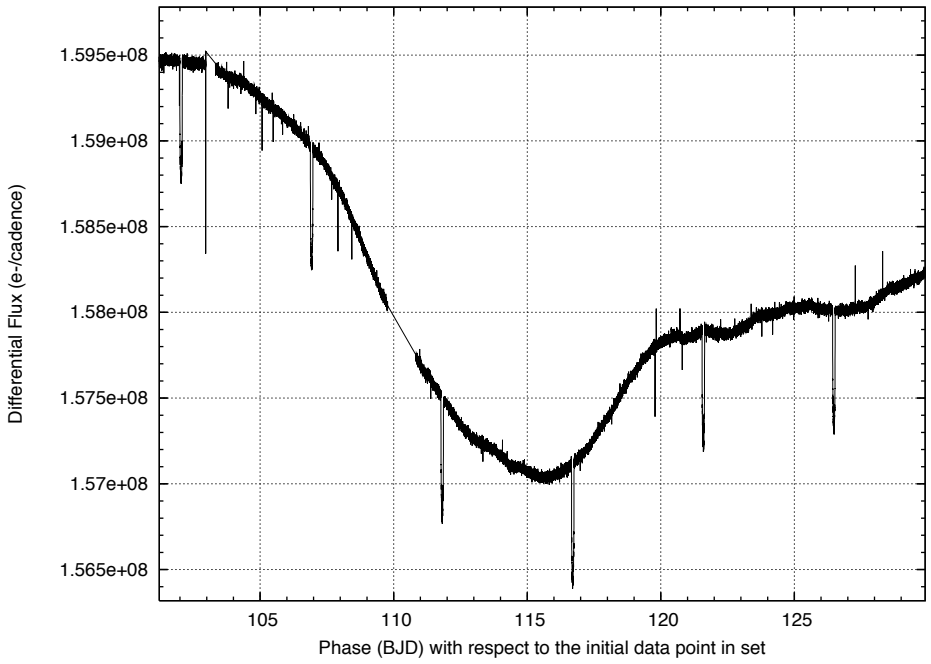

Figure 4.5 Transit #24 ($T_{trans} \approx 116.7$ in phase), is after the local minimum in the light curve, indicating a leading rather than trailing occultation

4.1.3 Spot constraint and degeneracy

One might imagine degenerate solutions of a small spot transited across a diameter resembling a grazing occultation of a relatively large spot. This degeneracy is easily broken when considering the overall light curve in concert with the transit signal. Consider the spot signal

detected in transit #16 for example. The occultation of this particular spot last ∼0.24 hours

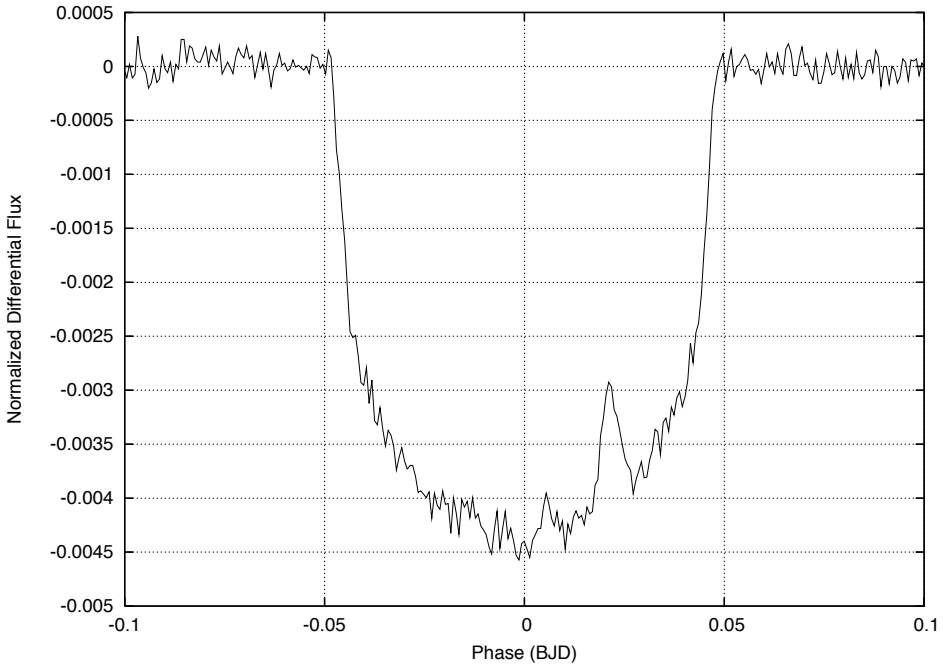

Figure 4.6 Phased, Normalized Transit #16

(the complete transit lasts 2.35 hours). Assuming that this were a transit across the diameter of the spot, this would imply a spot diameter of $\sim 3.0 \times 10^4$ km, using projected velocities $v_{p,x}$ = -33.1 km s^{-1} and $v_{s,x}$ = 1.24 km s^{-1} (the x-axis here is parallel to the equator of the star). The 're-brightening' signal expect from that size spot would be an ≈0.35% increase in flux, where the observed signal is only ≈0.11%. This means that this spot (or any other by example) is not subject to the "small spot diameter versus large spot chord" degeneracy. In order to reproduce this spot, you must increase the size of the spot, and increase the angle between the centers of the planet and the spot (make it a grazing eclipse). This problem would be more difficult to address, if spots were allowed more flexibility in their morphology and behavior, but for the purposes of this project, that level of detail is unnecessary.

Another possible degeneracy that was neglected in this analysis is the spot area vs. contrast ratio. This means that the same signal can be produced with a smaller spot and larger contrast

difference between spot and photosphere as with a larger spot and smaller contrast difference. For example, if the flux drop between spot and continuum were increased from the 64.2% used throughout the project to 75% (for an arbitrary single-spot scenario), this would result in a flux differential change $\frac{\Delta F}{F} = 0.24\%$. Using the flux drop of 64.2%, to produce the same signal the radius of the spot would have to increase by over 50%. This result is not surprising as the flux from the spot goes like the fourth power of the temperature, which will impose a larger quadratic change in the radius. Again, this discussion gives a sense of full disclosure into what was done to derive the presented results, but also what could have been different done that might have produced different results.

4.1.4 Spot drift, lifetimes and differential rotation

As mentioned earlier, and might be hoped, if a spot "lives" long enough, there is a chance that it will produce a signal in more than one transit. When treating transits as individuals, the spot(s) fixed in one transit are observed in a later (or earlier) transit. In the model, this means that after a certain period of time has elapsed, the geometry of the planet in orbit and spot on the star align once again to produce another spot-in-transit signal where it would be expected. If the spot signal is absent, early, late, or otherwise changed, then we know that the spot may evolve, or move. This could result from spot evolution, drift, or differential rotation of the star. Table 4.2 lists spots that, based on the model, should appear in more than one transit. The table also shows if the 'second-sight' modeled spot has an associated observed spot, and what this would imply about the necessary drift in longitude and latitude for any one modeled spot to be clearly identified as having more than one occurrence in the data.

For 'second-sight' spots in which there is no associated spot in the data, the drift in longitude can be estimated by considering how far it had to drift away for it *not* to be seen. Nothing can be said for the drift of latitude of these particular spots, because for a fixed longitude, a realistic change in latitude would still be observed in the later (or earlier) transit. For 'second-sight' spots observed in a later transit with multiple signals in the data, the drift calculations are only carried out for what would be the best candidate for multiplicity. Spots that are doubly 'second-sighed' (i.e. spot #1 observed in spot #20 and spot #20 observed in spot

#1 - each independently) are marked with an asterisk in their transit identification number. The consistency in the time difference between multiple observations of a modeled spot is not surprising, as 29.3 days $\approx 6P_{orb}$, 92.9 days $\approx 19P_{orb}$, and 122.2 days $\approx 25P_{orb}$.

It is not difficult to eliminate many pairs in this list from being genuine same-spot candidates. Any spot combination where a very large drift in latitude is required is very unlikely. On the Sun, over a period of 5.5 years active regions tend move in latitude towards the equator with an average change of $\sim 30^\circ$ over that time period. HAT-P-11 is not like the Sun, but it is unexpected that such a drastic difference in properties would be observed, especially when they have similar rotation velocities. Also, spots do not cross the equator of the Sun. As will be shown below, this is also a very unlikely scenario for the spots on HAT-P-11, as it may not be like the Sun in many ways, they show several distinctive phenomenological similarities in the average geography of their active regions.

The best candidates for making an argument towards recurrence would be spot 19a $\rightarrow$ spot 25a, spot 22 $\rightarrow$ spot 16, spot 27 $\rightarrow$ spot 21, and spot 28b $\rightarrow$ spot 22. Each pair has a latitude drift lat $< 5^\circ$ and a longitude drift of long $< 15^\circ$. An immediate caveat with three for the four pairs is that they are anti-causal. The initial spot was fixed at a later time than where they are observed a second time. This is a symptom of the spots in the model being permanent. Interestingly, each possible combination is separated by the same amount of time, ~ 6 P_{orb} which is very close to a 6:1 resonance between the orbital period of the planet and the rotation period of the star.

The average (absolute) distance in latitude from the equator for each spot candidate is 23.6°. This supports the possibility of these longitudinal drift measures being a function of latitude as it is on the Sun (higher latitude spots will have a slower rotation period than those near the equator), where in these special cases the longitudinal drift is always larger than that in latitude. Also supporting the evidence of possible differential rotation, is that in three of four primary candidates (excluding spot 22 $\rightarrow$ spot 16) the latitudinal drift is towards the equator of the star. Assuming causal order, if spot 28b is fixed to the star and observed in transit 22 in the model, then it must also be identified as spot 16 being observed again in transit 22. From this frame of reference, the above latitude drift observation holds true.

Differential rotation could also be argued solely from the shape of the out-of-transit light curve as a whole. Between the dominant, primary minima and maxima, there appears to be some possibly non-periodic behavior, or rather an envelope of more than one period being present as spots are carried across the stellar disk. The light leading up towards the first primary maximum (in the first 13 days of the data) looks suspiciously like the light leading up towards the final maximum. Of course, more data would help address this odd behavior.

This unusual behavior in the light between primary minima could be explained by short-lived spots growing and decaying at different phases in the rotation, which could be supported by the fact that so few of the observed spot transits on the star show the possibility of being repeat spots, and how the several of the best candidates for recurrence are measured individually with different radii. The static nature of the spots in the simulation is an obvious deficiency, but that will be left for the next person to tackle.

4.2 Determining stellar inclination

There appears to be two broad preferential regions in which spots are occulted by the planet. With the orbit of HAT-P-11b as it is (nearly polar), these two regions in the transit correspond to two different ranges in latitude on the surface of the star. If the rotational axis is inclined at the adopted value of 88.5°, then these regions are apparently asymmetric about the equator. If we assume that HAT-P-11 has a symmetric pattern of activity about its equator, exactly as observed on the Sun (the basis of the Butterfly diagram), then this could be the same phenomenon observed in Figure 4.7. This would explain the latitude-dependent activity strips, but not the apparent asymmetry about the equator, given that i is so high. But the inclination has been assumed to be near 90° simply because it must be to have such large transit signatures.

So if HAT-P-11 is assumed to have active latitudes, the asymmetry in the observed latitudes about the equator can be explained as an incorrect input stellar inclination. The average, unweighted latitude derived of all spots above the equator is +10.6° and the derived average for all spots below the equator is -27.6°. The average of these two numbers is 19.1°. So if the lower hemisphere active latitude were moved 8.5° towards the equator, and the upper

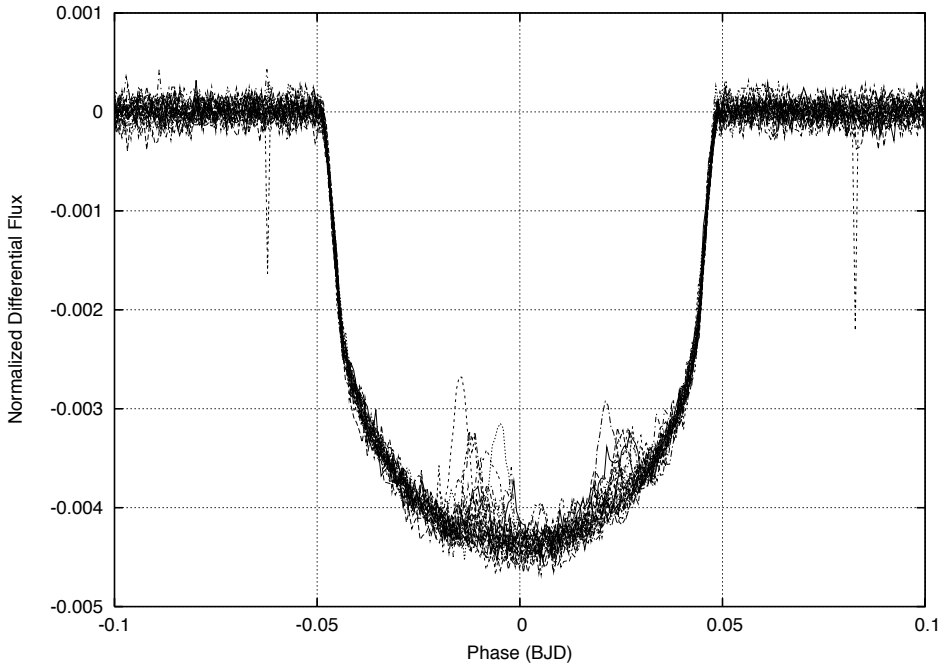

Figure 4.7 This figure shows all but one of the 26 transits in the data set (phased and normalized) overlaid on top one another.

hemisphere active latitudes were moved 8.5° away from the equator, the symmetry of alignment would show active latitudes at ± 19.1°. This movement of latitudes is achieved by increasing the stellar inclination. Adding 8.5° to the input inclination angle shows that the actual inclination should be 88.5° - 8.5° = 80°, which means that the star is tilted 10° towards the observer. So by modeling this system using the technique of transit mapping, we have also measured the stellar inclination axis. This result is supported by the Rossiter-McLaughlin measurements which derived the spin-orbit angle λ, as only a net blueshift was measured through the duration of each transit, meaning that from our frame of reference, the transiting planet never covers any part of the star that is rotating towards the observer, or at least it does for an unmeasurable length of time to detect.

4.3 From spots to map

Changing the stellar inclination axis likewise changes each quoted spot latitude. Spots in the southern hemisphere must be moved closer to the equator by 8.5° and spots in the northern hemisphere must be moved away from the equator by 8.5°. The richness of this system is double-edged however. Due to the inability to unequivocally identify the starspots as individuals, and their tendency for very dynamic behavior, our model has proven insufficient to completely characterize the length of data available for analysis. The demon of all astronomers is that of not enough data, and he has prevailed yet again. What has been identified are two distinct active latitudes on HAT-P-11, as well as individual inhomogeneities on its surface with a sub-degree precision. Evidence and arguments for differential rotation on the surface of the star has also been presented. A feature that will have to be included for future analysis of this system.

Table 4.1 Spot Parameter Results

Spot-in-transit #	Radius (10^4 km)	Latitude (°)	Longitude (°)
1	5.0 ± 0.08	-21.4 ± 0.26	306.7 ± 0.26
3	3.18 ± 0.12	+18.6 ± 0.41	188.5 ± 0.41
5	6.9 ± 0.06	+7.4 ± 0.19	89.0 ± 0.19
6	3.6 ± 0.11	-19.2 ± 0.36	33.9 ± 0.36
8	5.0 ± 0.08	+14.0 ± 0.26	258.8 ± 0.26
11a	3.7 ± 0.10	+12.0 ± 0.35	86.8 ± 0.35
11b	3.8 ± 0.10	+2.3 ± 0.34	89.0 ± 0.34
11c	3.5 ± 0.11	-34.5 ± 0.37	98.6 ± 0.37
12	4.2 ± 0.09	-23.5 ± 0.31	-23.5 ± 0.31
14a	9.4 ± 0.05	+19.1 ± 0.14	292.9 ± 0.14
14b	4.0 ± 0.10	-33.7 ± 0.32	285.3 ± 0.33
16	3.8 ± 0.10	-26.9 ± 0.34	170.7 ± 0.34
18a	4.0 ± 0.10	+11.5 ± 0.32	45.7 ± 0.32
18b	3.7 ± 0.10	+3.5 ± 0.35	47.7 ± 0.35
19a	5.5 ± 0.07	+12.0 ± 0.24	0.7 ± 0.24
19b	3.3 ± 0.12	-34.0 ± 0.39	11.1 ± 0.40
20	5.7 ± 0.07	-36.2 ± 0.23	319.6 ± 0.23
21	3.2 ± 0.12	-32.0 ± 0.40	244.4 ± 0.41
22	6.1 ± 0.07	-28.6 ± 0.21	181.8 ± 0.21
23a	6.2 ± 0.07	+12.9 ± 0.21	133.7 ± 0.21
23b	3.9 ± 0.10	-28.9 ± 0.33	140.6 ± 0.33
24	4.0 ± 0.10	+15.6 ± 0.32	73.1 ± 0.33
25a	3.5 ± 0.11	+8.2 ± 0.37	13.7 ± 0.37
25b	3.7 ± 0.10	-30.5 ± 0.35	26.3 ± 0.35
26	3.2 ± 0.12	+16.4 ± 0.40	315.0 ± 0.40
27	4.8 ± 0.08	-30.0 ± 0.27	256.6 ± 0.27
28a	4.8 ± 0.08	+19.0 ± 0.27	203.4 ± 0.27
28b	5.9 ± 0.07	-27.3 ± 0.22	196.3 ± 0.22

Table 4.2 Spot drift estimates for modeled spots observed in more than one transit

Fixed spot #	'second-sight' #	spot in data?	ΔTime (days)	ΔLat (°)	ΔLong (°)
1*	20*	Yes	92.9	14.8	12.9
5*	24*	Yes	92.9	8.2	15.9
8	27	Yes	92.9	44.0	2.2
14a	1	Yes	63.5	40.5	13.8
14a	20	Yes	29.3	55.3	26.7
19a	25a	Yes	29.3	3.8	13.0
19a	25b	Yes	29.3	42.5	24.6
20	26	Yes	29.3	52.6	4.6
22	16	Yes	29.3	1.7	11.1
23a	4	No	92.9	-	$\gtrsim$11.7
23b	4	No	92.9	-	$\gtrsim$3.6
25b	6	Yes	92.9	11.3	7.6
27	2	No	122.2	-	$\gtrsim$6.6
27	21	Yes	29.3	2.0	12.2
28a	9	No	92.9	-	$\gtrsim$5.7
28b	3	Yes	122.2	45.9	7.8
28b	22	Yes	29.3	1.3	14.5

CHAPTER 5. Summary and discussion

The goal of this project was to determine the spatial and temporal coverage of surface inhomogeneities on the active star HAT-P-11. Although an unambiguous solution could not be achieved through the presented analysis, the overall goal was met in that surface features were individually parameterized and the analysis technique allowed for some unexpected results, particularly a measure of the stellar inclination axis and an observation of differential rotation on the surface of the star.

5.1 Why does this method work?

The method of transit mapping works because the characteristic bump in a transit as the planet occults a starspot is easily measurable with the high-precision, high-cadence photometry provided by *Kepler*. For many exoplanetary astronomers, these signatures are more troublesome than beneficial, as they can make transit timing variation measurements (a means to discover additional bodies in a system) very difficult. But for spot-modelers, having a measure of coverage from both in and out-of-transit light provides a level of constraint unachievable through by any other photometric means.

The model also determines why this method works. If we were unable to accurately enough reproduce the data characteristics of *Kepler*, the odd geometry of the system, and physical phenomena such as limb-darkening and velocity gradients, then the conclusions drawn from the analysis would be superficial at best. We were able to reach a level of accuracy with the model to draw realistic conclusions from its results, and in the process pointed out how future attempts to characterize this system can be improved by including effects not in our model (such as differential rotation).

5.2 Understanding the importance of this project

Studying systems like HAT-P-11 with its planet HAT-P-11b are important because of the broad range of astrophysical insight such systems can provide to astronomers here on Earth. This thesis has focused almost entirely on the surface of the star, but this was only possible from previous discoveries, notably the drastic spin-orbit misalignment of the planet. This misalignment is telling of the history of this system, as the most popular theory describing how HAT-P-11b settled into a near-polar orbit was from a significant scattering event with another body in the system. While the scattering event probably had apocalyptic consequences for the inhabitants of HAT-P-11b, it has given the exoplanetary science community here on Earth an in-depth look into the richness of the system, unavailable with the more common equatorial plane orbital path of most planets. The dynamic history of planet formation and further evolution is a cutting-edge field currently, a focus that will have a wealth of statistics available from the analysis of the ∼1200 planetary candidates discovered by *Kepler* alone. Studying the frequency and history of solar systems outside our own will provide insight into whether or not a system where intelligent life could manifested itself is rare or common in the Galaxy.

Aside from the interesting relationship between the planet and host star, deriving information about stellar activity is important to the population on Earth, because activity levels on the Sun directly affect our climate, and predicting outbursts like solar flares or coronal mass ejections can help protect our dense space-based infrastructure of communication and GPS satellites. The cyclic nature of activity on the Sun has been well documented and attempts to model this behavior improve from year-to-year, so our knowledge of the driving forces of activity on the Sun can be used as a template for activity on other stars. Better physics behind the magnetic fields inside stars will better constrain stellar models, which will in turn increase the knowledge base of stellar astrophysics as a discipline.

What my project can contribute to this knowledge base, is an example of a star where using information derived from the influence of starspots, we have determined rotation period, inclination, location of active latitudes, and overall coverage of spots on the surface of the star. The rotation period is strongly coupled to levels of activity on stars with a convective envelopes

and the presence of active latitudes indicate that HAT-P-11 may have similar periodic behavior like that observed on the Sun. The prospect of developing a 'butterfly diagram' for a star other than our own is a genuine possibility with the quality and quantity of data collected by *Kepler*.

5.3 Summary

What we find is that the activity on the surface of HAT-P-11 tends to follow a similar pattern as that observed in the surface of the Sun. This is a promising result, as popular theory suggests that all stellar activity is driven by a common dynamo mechanism. This pattern could also be indicative of the age of the star, as younger stars will rotate faster, and their surface activity should show less order. Although we could not define the exact temporal behavior of the individual spots modeled in this work, their instantaneous radii, longitudes and latitudes were all well constrained, effectively 'seeing' the surface of another star. The possibility of spot drift in longitude and latitude was addressed, likely a symptom of differential rotation on the surface of the star, but could not be definitively confirmed. While we had the capability to include spot growth and decay into our model, the lack of a clear example for any one spot observed in more than a single transit prevented their implementation into the analysis. As more data become available, the accuracy to which you could predict the system behavior would increase, and a more refined model will be able to include more subtle effects.

HAT-P-11 is undoubtedly a rich system, and we have only scratched the surface with this project. The goal for the next iteration of this study should be to take the framework laid out here, and use it to address such issues as differential rotation with latitude, temporal spot size behavior, stellar age versus activity pattern, missing spots, possible flare-spot associations, among many others. There is also opportunity to refine the parameters of HAT-P-11b. How might its evolution be altered by the unusual orbit it follows? This thesis has shown interesting and important results for stellar variability driven by starspot modulation, but further analysis, hopefully with an expanded data set, has the capability to characterize this system to an unmatched level of precision and accuracy.

APPENDIX A. Additional material

Observed transits

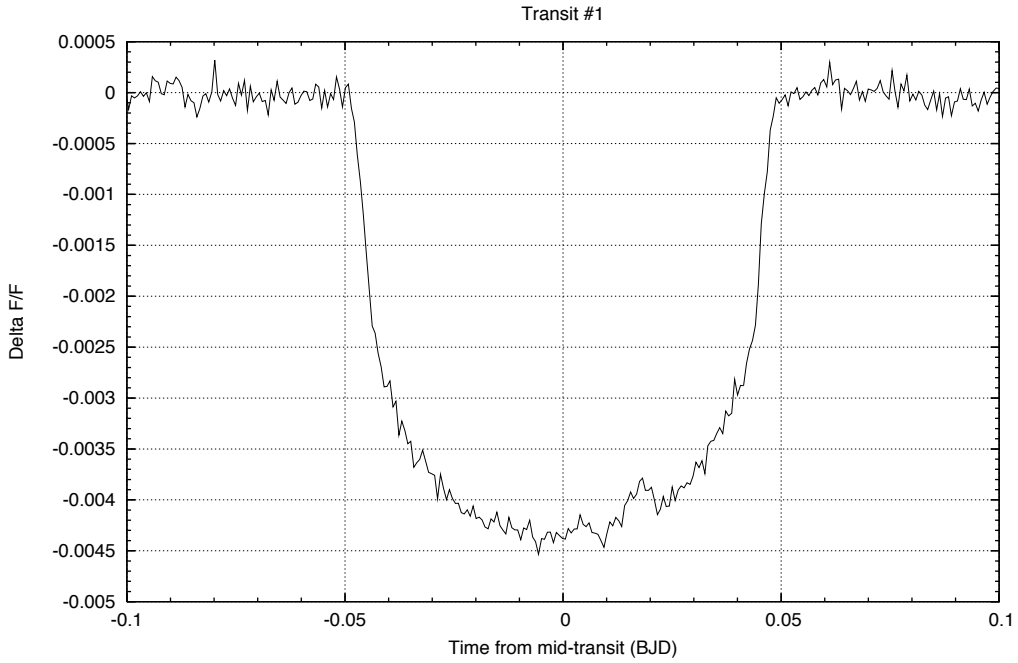

Figure A.1 Transit 1

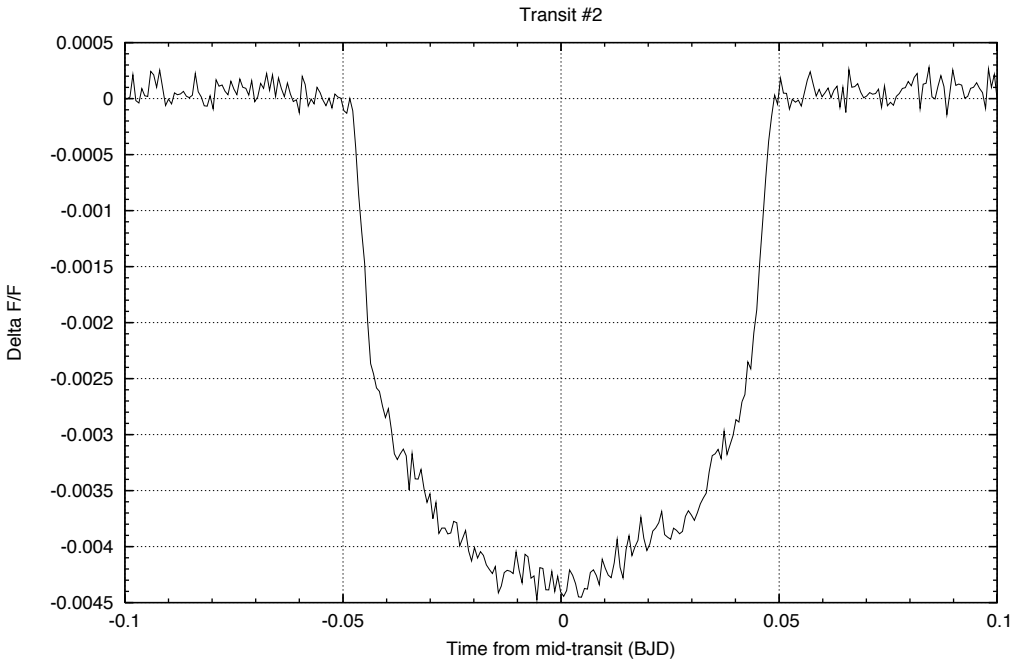

Figure A.2 Transit 2

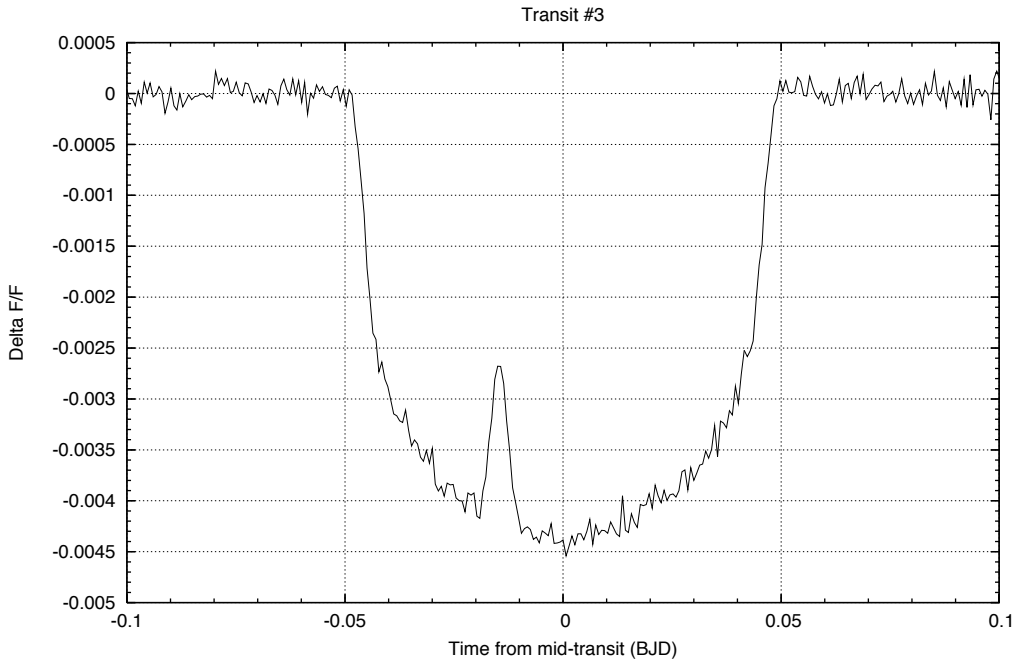

Figure A.3 Transit 3

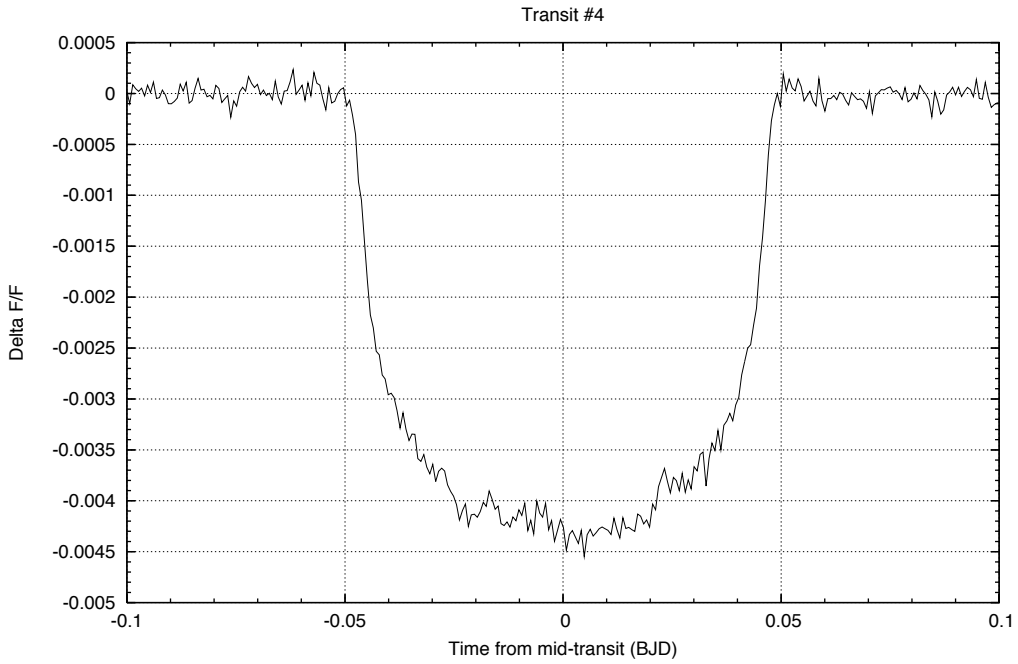

Figure A.4 Transit 4

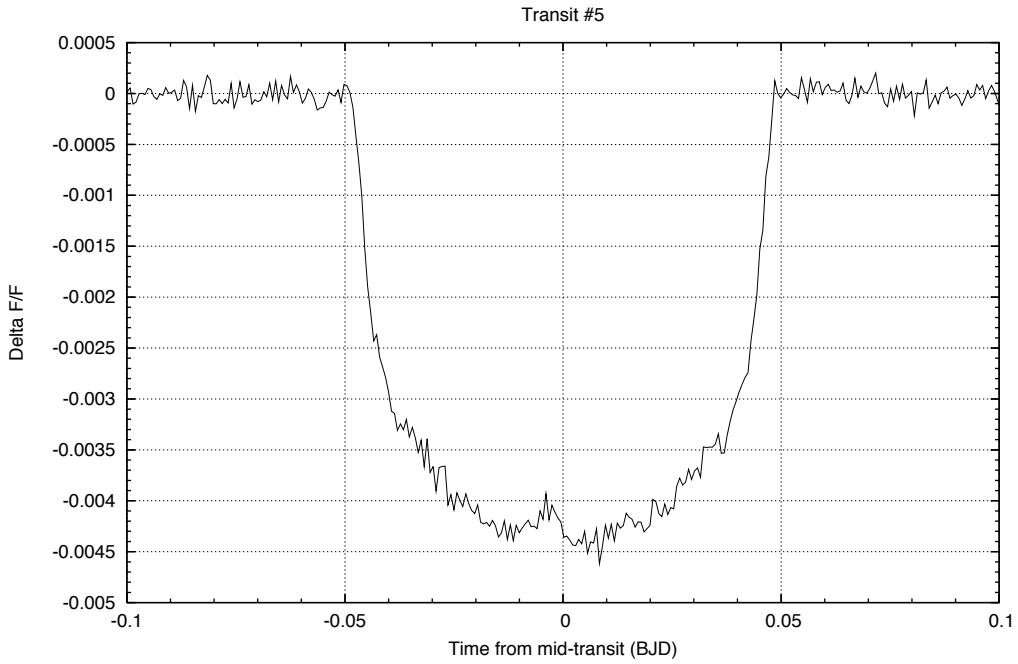

Figure A.5 Transit 5

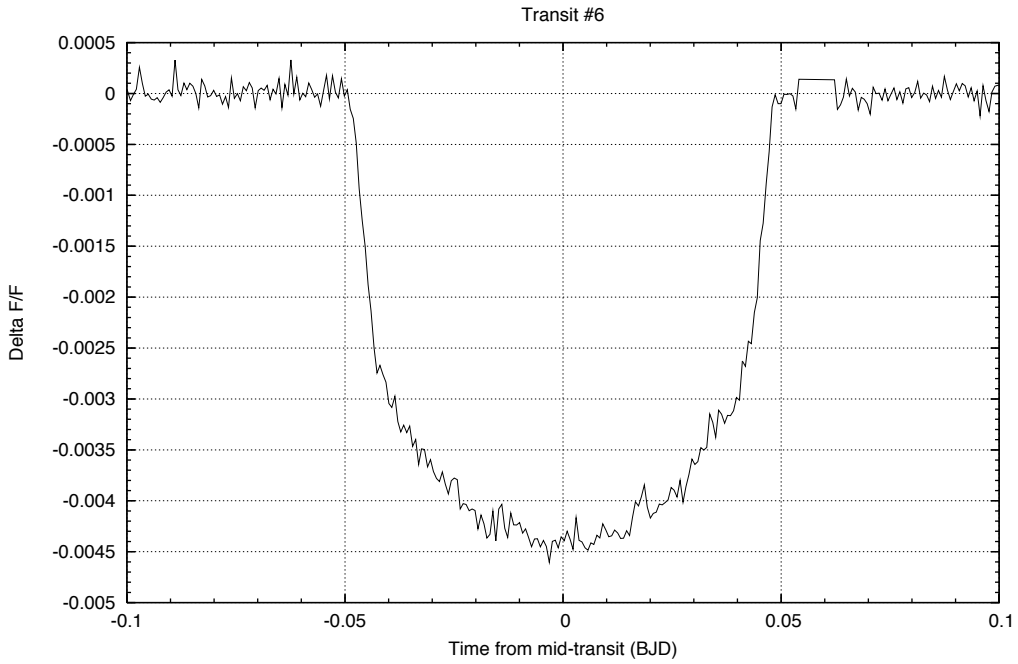

Figure A.6 Transit 6

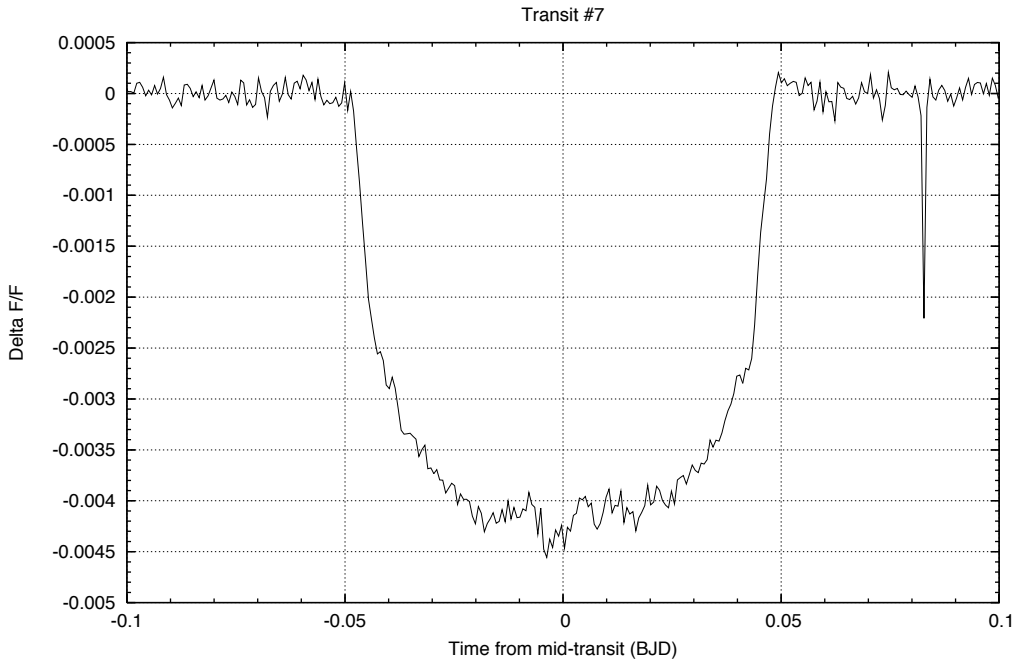

Figure A.7 Transit 7

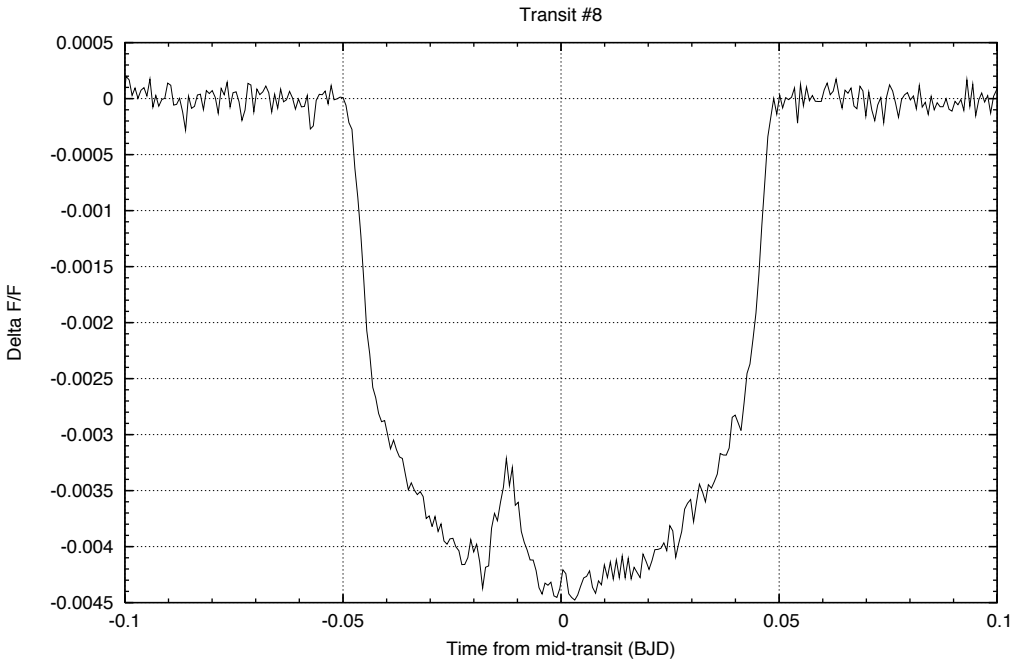

Figure A.8 Transit 8

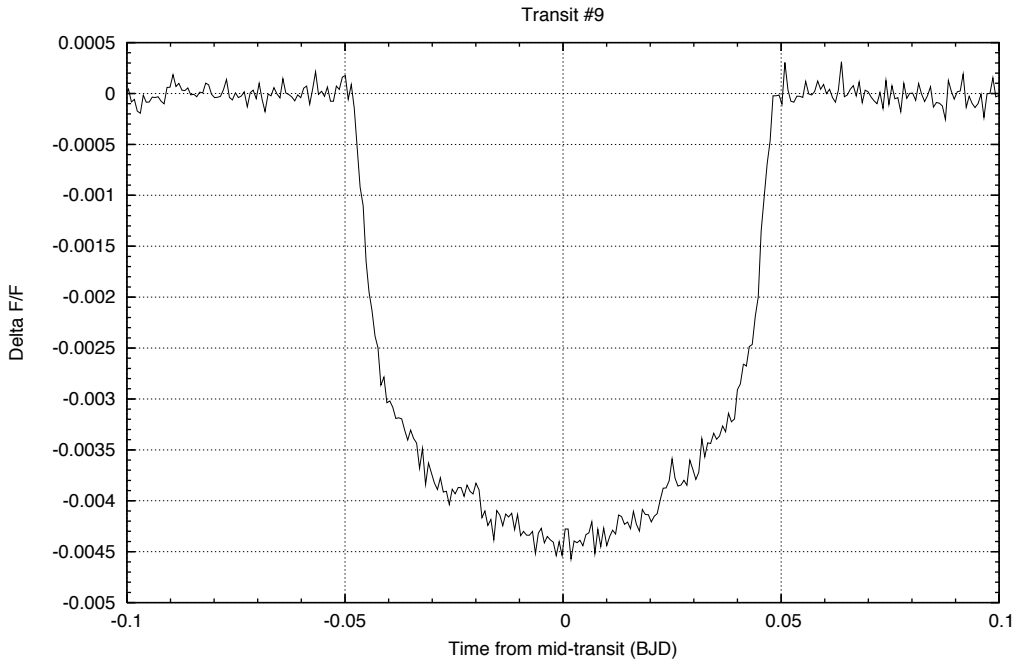

Figure A.9 Transit 9

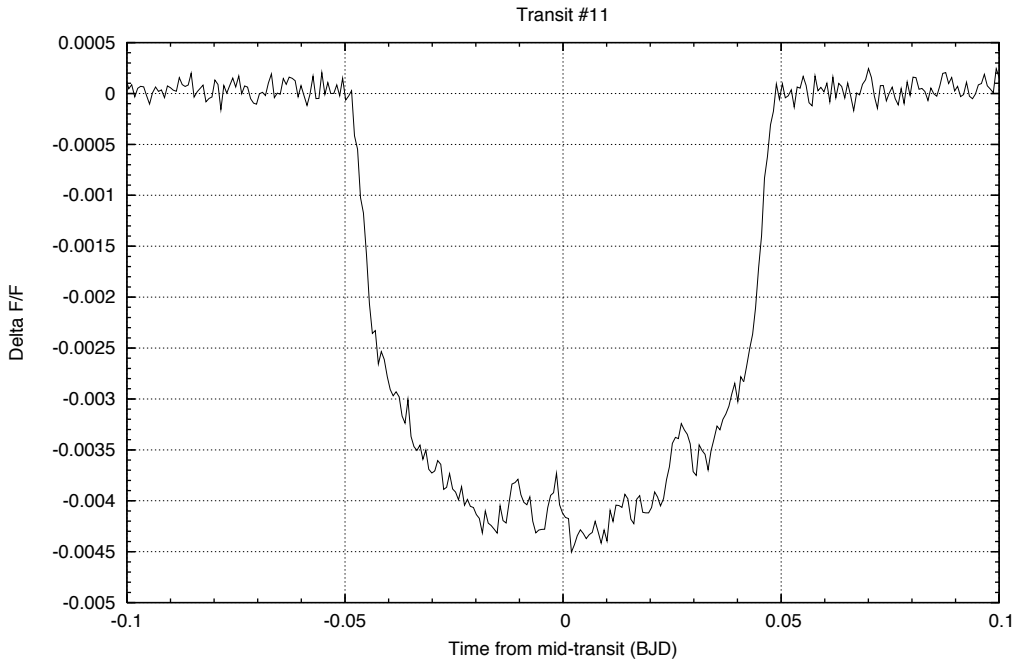

Figure A.10 Transit 11

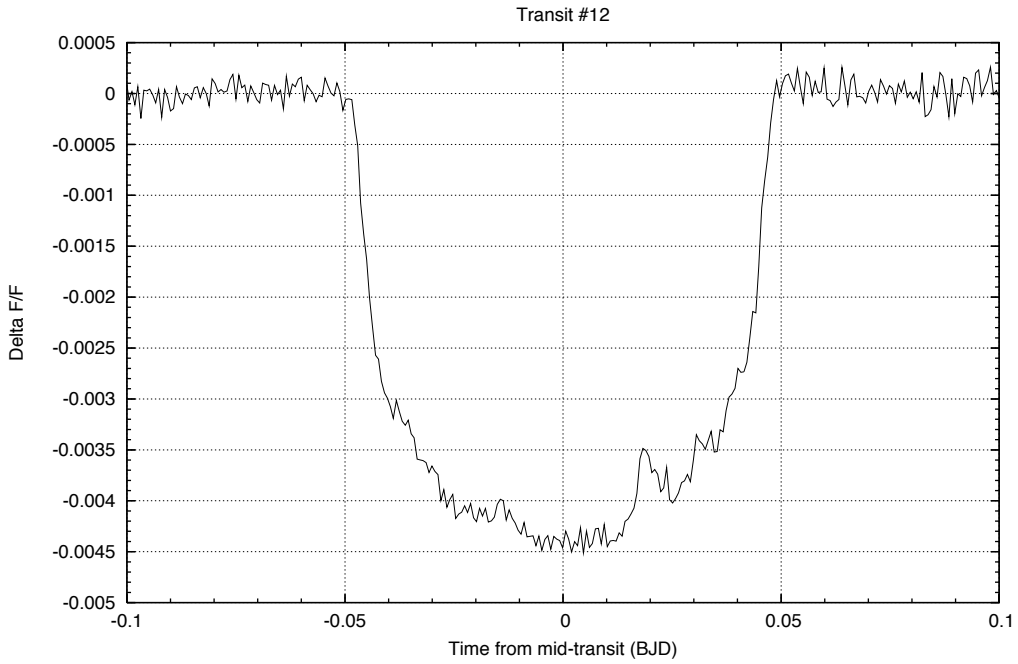

Figure A.11 Transit 12

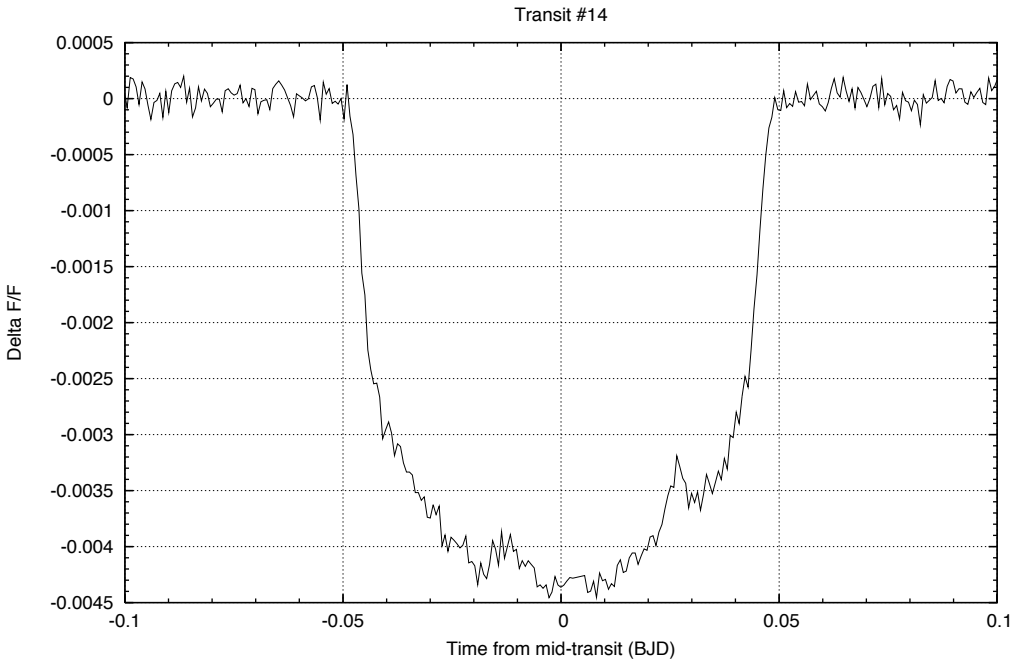

Figure A.12 Transit 14

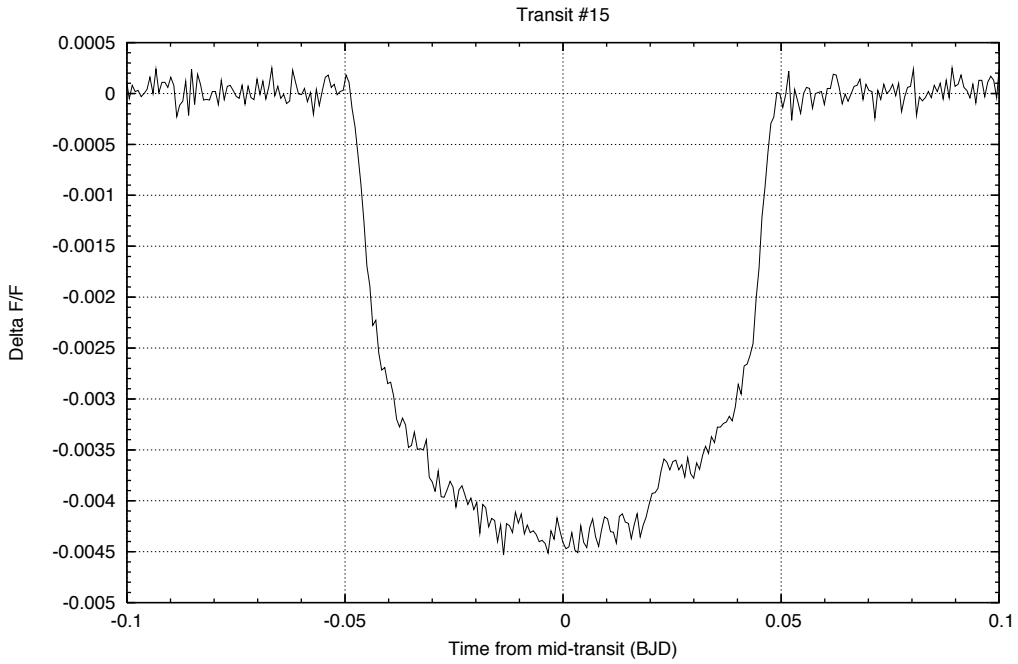

Figure A.13 Transit 15

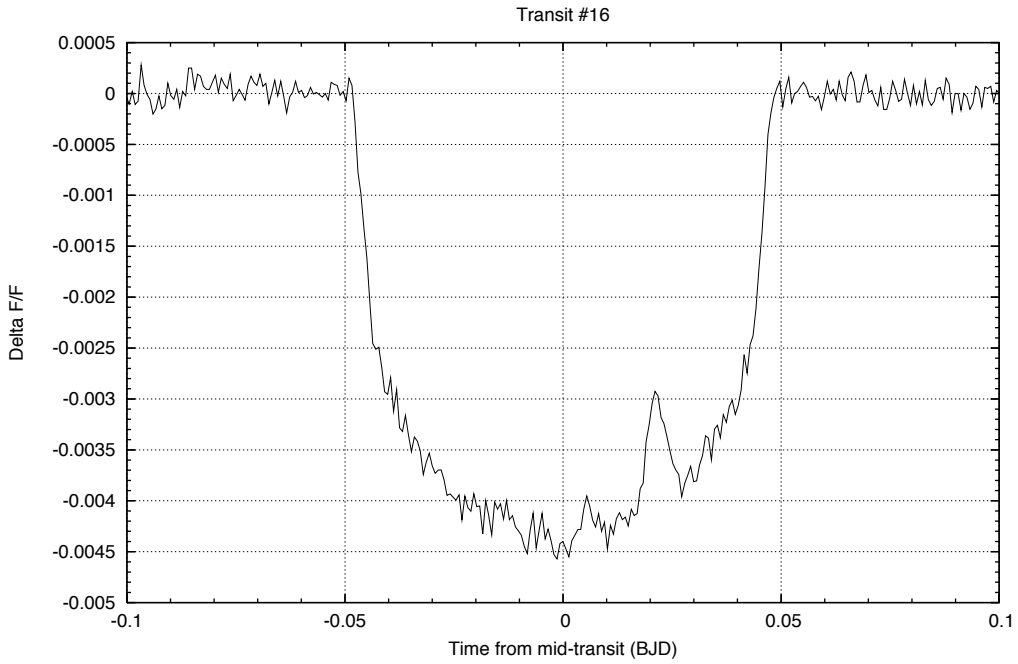

Figure A.14 Transit 16

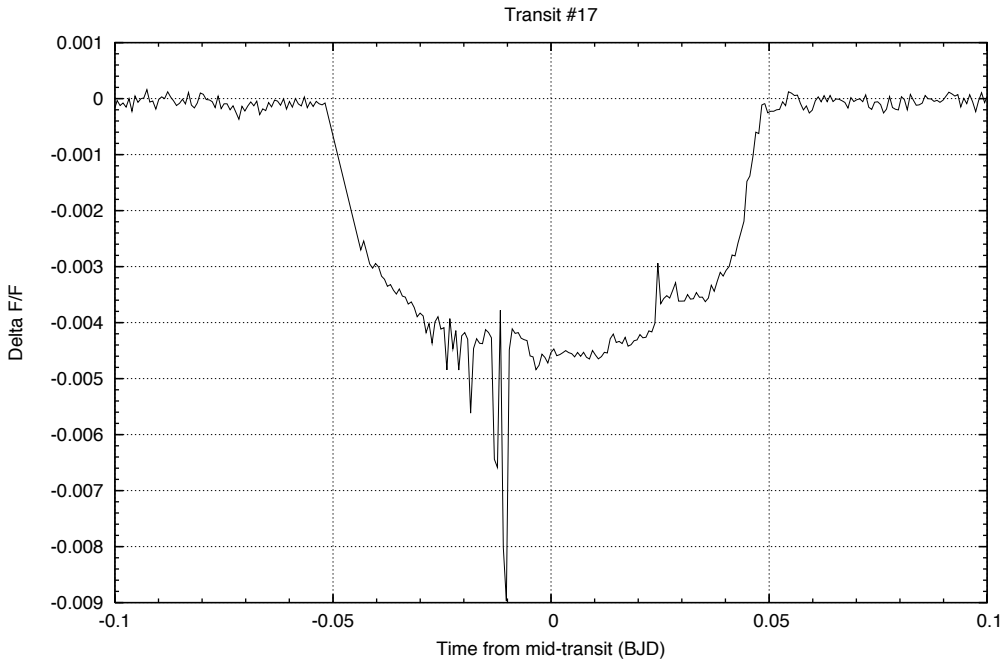

Figure A.15 Transit 17

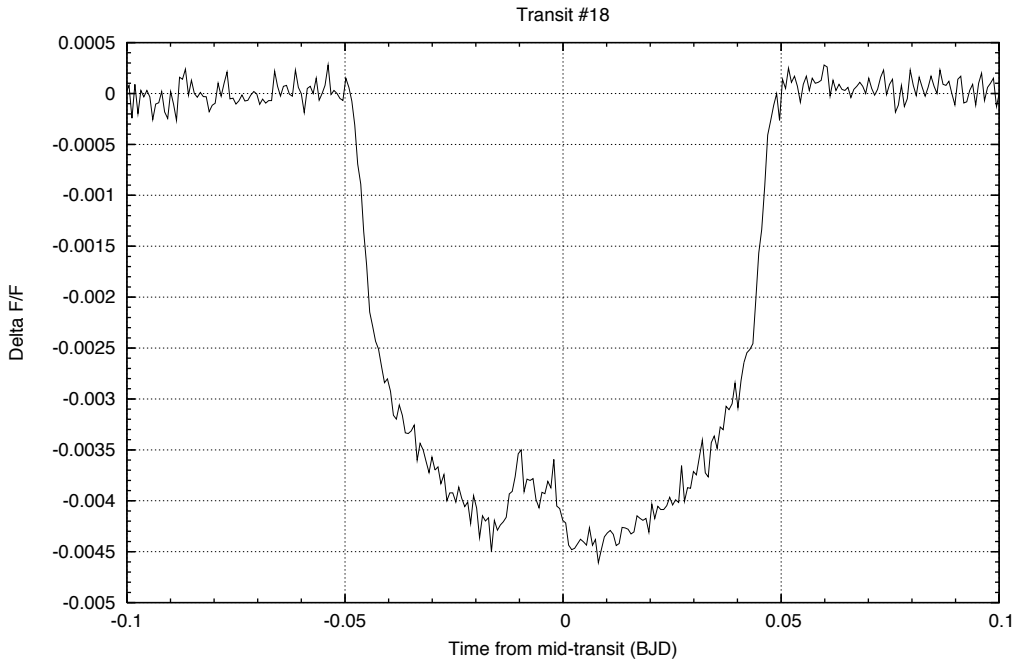

Figure A.16 Transit 18

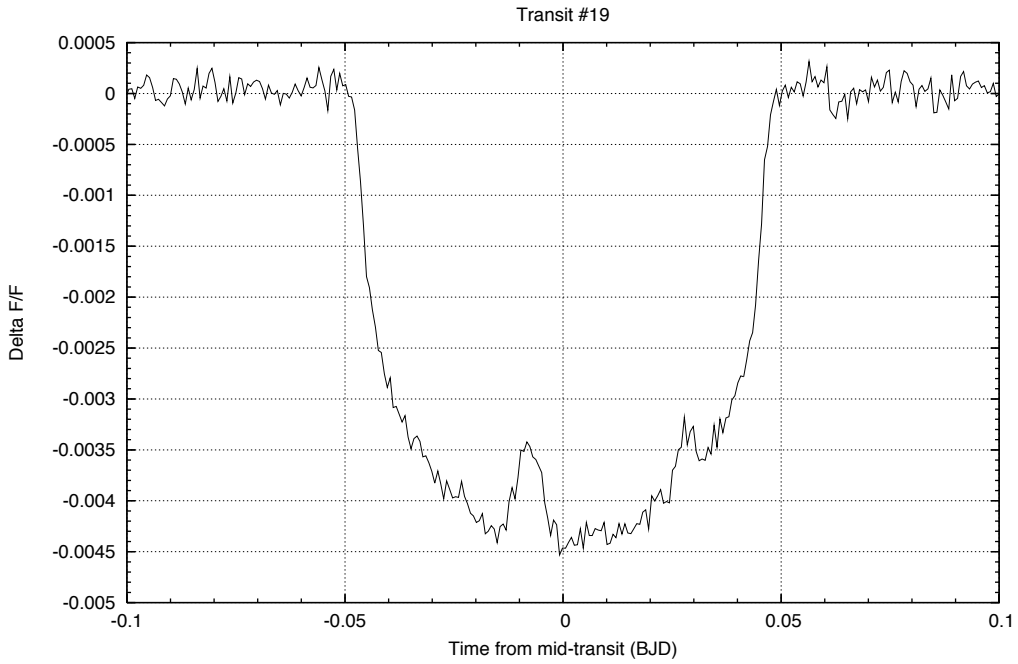

Figure A.17 Transit 19

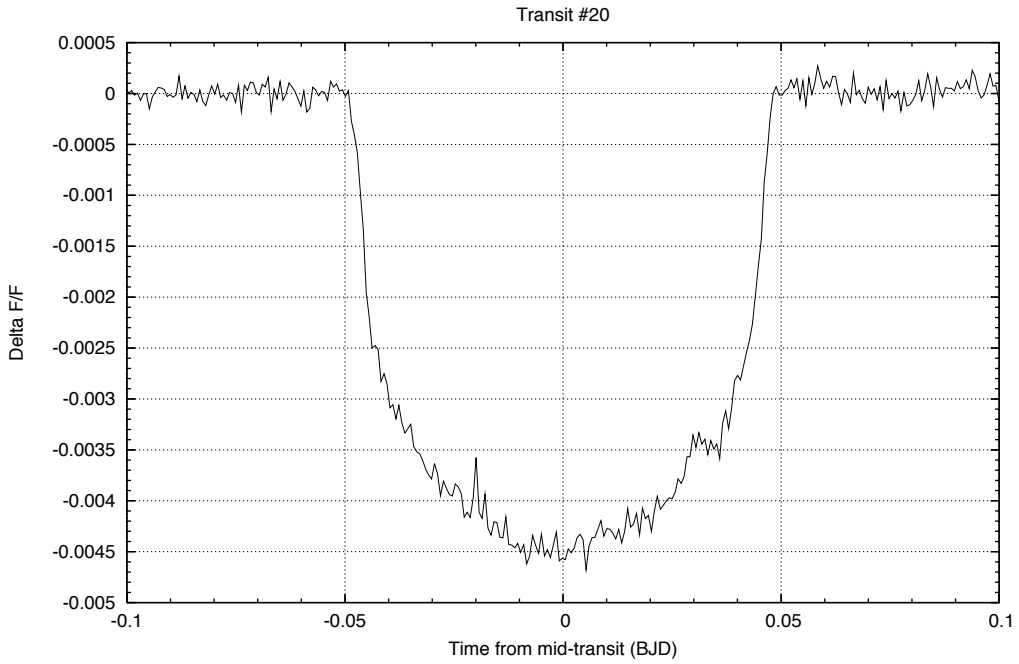

Figure A.18 Transit 20

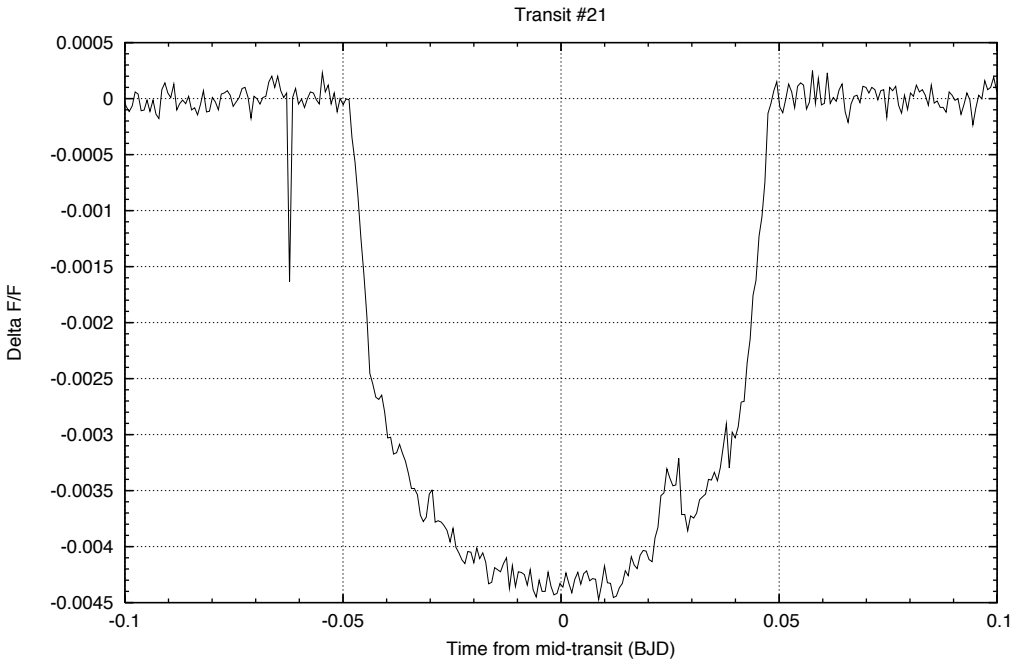

Figure A.19 Transit 21

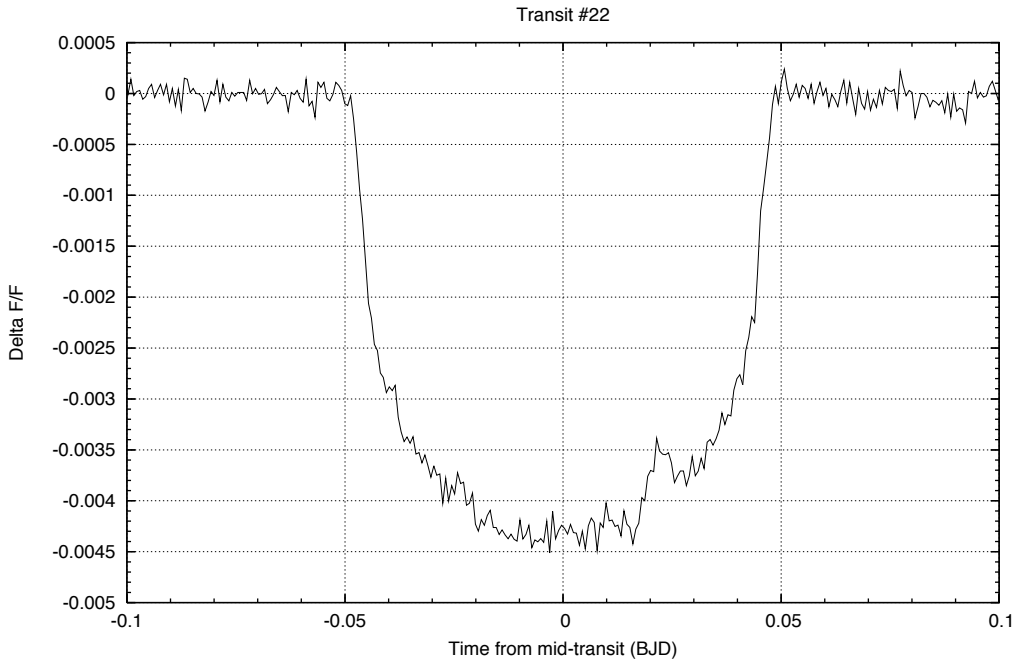

Figure A.20 Transit 22

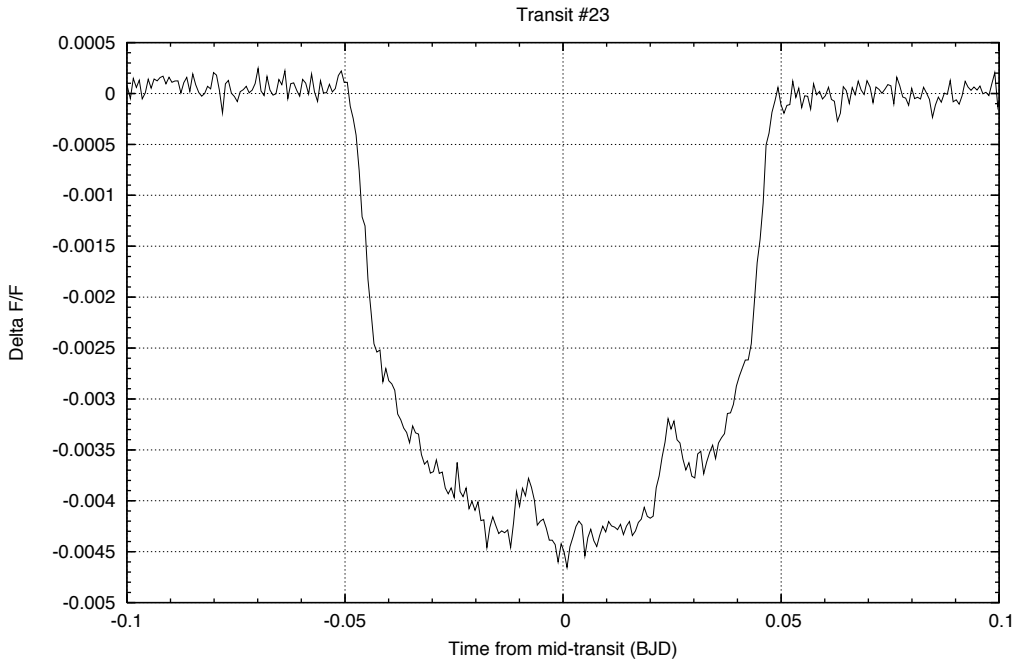

Figure A.21 Transit 23

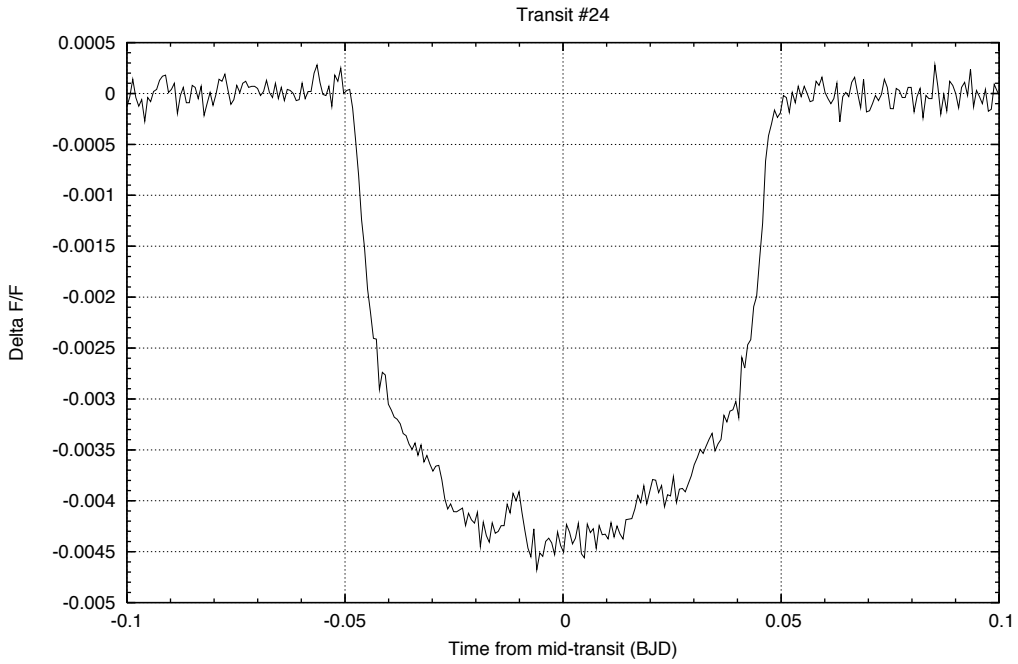

Figure A.22 Transit 24

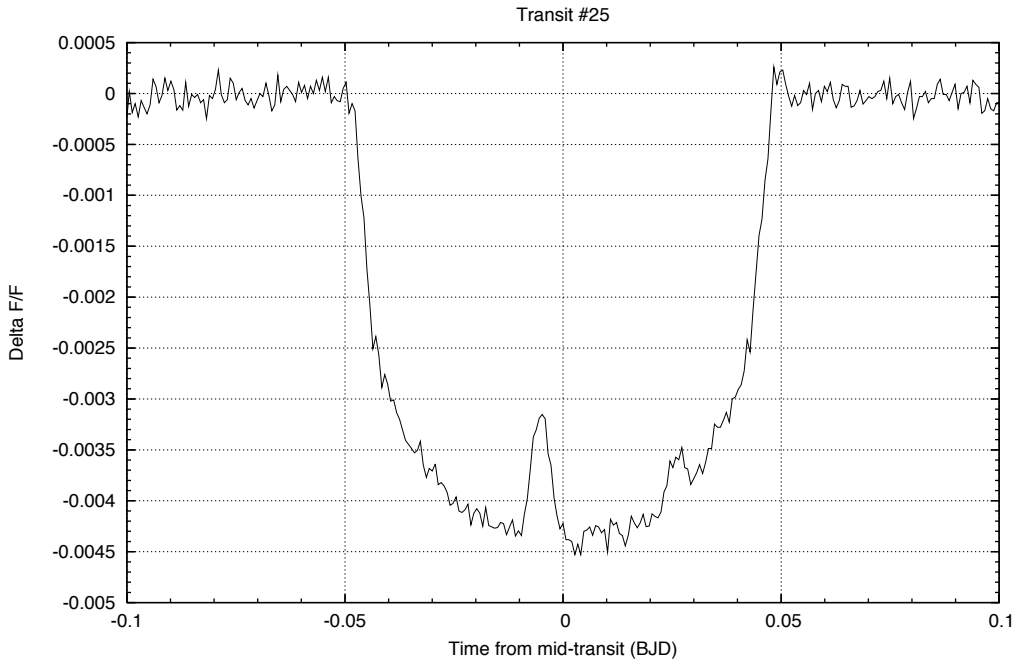

Figure A.23 Transit 25

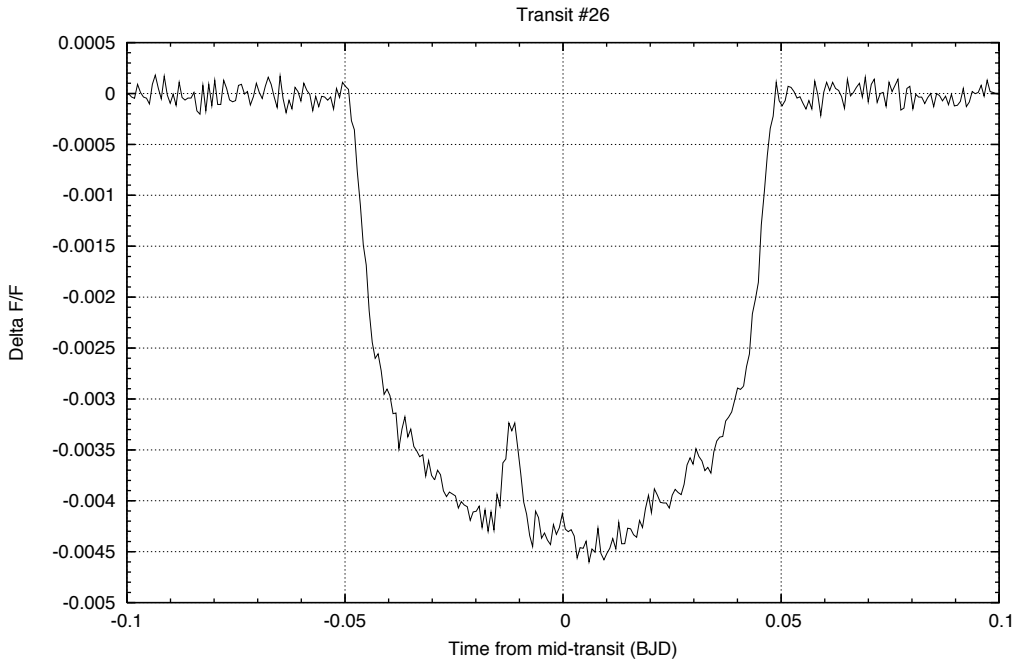

Figure A.24 Transit 26

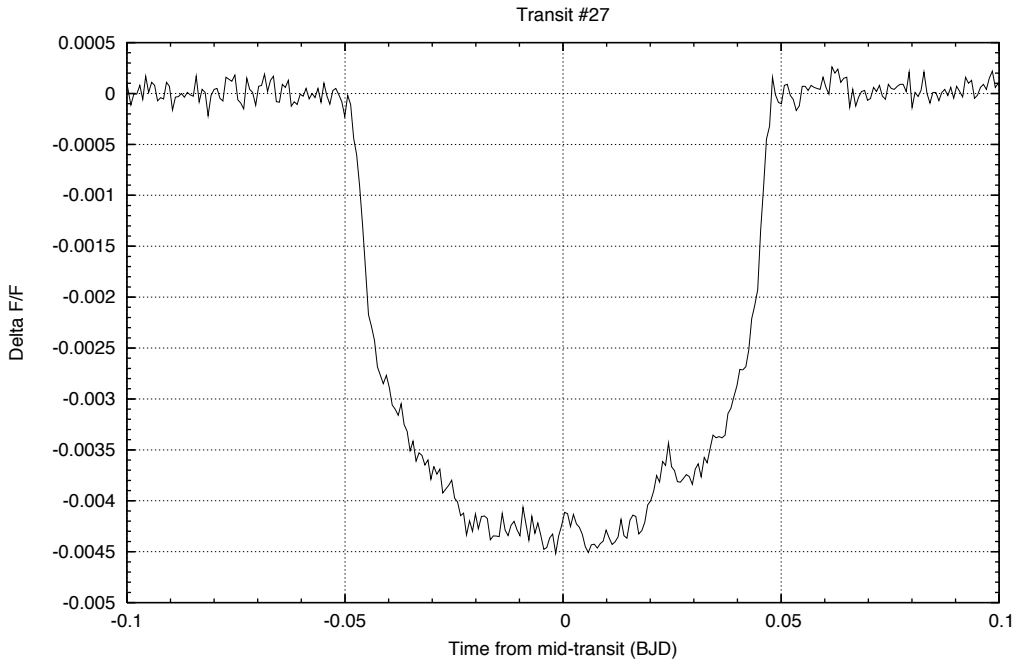

Figure A.25 Transit 27

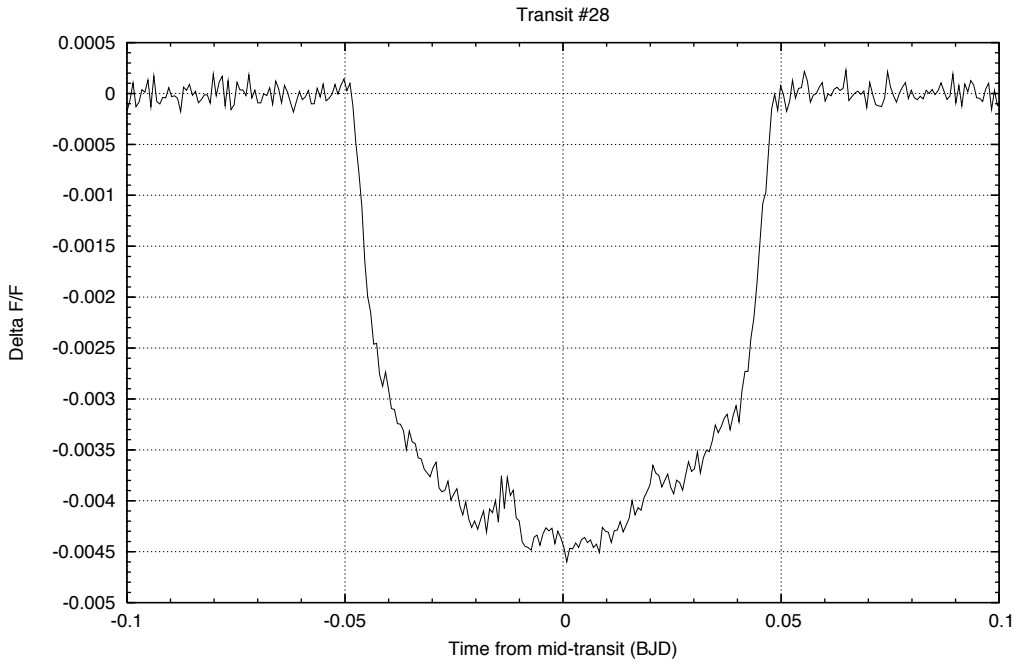

Figure A.26 Transit 28

BIBLIOGRAPHY

[Auvergne et al. 2009] Auvergne, M. et al, 2009, *A&A*, **506**, 411-424

[Bakos et al. 2010] Bakos, G. *Á*., 2010, *AJ*, **710**, 1724-1745

[Baraffe et al. 2008] Baraffe, I., 2008, *A&A*, **482**, 315

[Berdyugina 2005] Berdyugina, S.V., 2005, *LRSP*, **2**

[Borucki et al. 2010] Borucki, W.J. et al., 2010, *Science*, **327**, 977

[Borucki et al. 2003] Borucki, W.J. et al., 2003, *ASP Conference Series*, **294**, 427-440

[Carroll & Ostlie 2007] Carroll, B.W. and Ostlie D.A., 2007, An Introduction to Modern Astrophysics 2nd Ed., San Francisco: Pearson Education, Inc., publishing as Addison-Wesley

[Charbonneau et al. 2000] Charbonneau, D., Brown, T., Latham, D.W. and Mayor, M., 2000, *ApJ*, **529**, L45-L48

[Claret 2004] Claret, A., 2004, *A&A*, **428**, 1001-1005

[Cowling 1981] Colwing, T.G., 1981, *Ann.Rev.Astron.Astrophys*, **19**, 115-135

[Emerson 1830] Emerson, R.W., 1830, *Journals*

[Galilei 1613] Galilei, G., 1613, *Rome - The Warnock Library*.

[Garćia et al. 2011] Garćia, R.A. et al., 2011, *MNRAS*, **414**, L6-L10

[Gilliland & Dupree 1996] Gilliland, R.L. and Dupree, A.K., 1996, *ApJ*, **463**, L29

[Gilliland et al. 2010] Gilliland et al., 2010, *ApJL*, **713**, L160-L163

[Hansen et al 2004] Hansen, C.J., Kawaler, S.D. and Trimble, V., 2004, Stellar Interiors: Physical Principals, Structure, and Evolution 2nd Ed, *NewYork* : *Springer*.

[Herschel 1795] Herschel, W., 1795 *Phil.Trans.Roy.Soc.Lond*, **85**, 46

[Hog et al. 2000] Hog, E. et al. 2000, *A&A*, **355**, L27-L30

[Kawaler & Veverka 1981] Kawaler, S.D. and Veverka, J., 1981, *JRASC*, **75**, 46

[Kjeldsen & Bedding 1995] Kjeldsen, H. and Bedding, T.R., 1995, *Astron.Astrophys.*, **293**, 87-106

[Koch et al 2010] Koch, D.G. et al., 2010, *ApJL*, **713**, L79-L86

[Maunder 1904] Maunder, E.W., 1904, *Mon.Not.Roy.Astron.Soc.*, **64**, 747

[McLaughlin 1924] McLaughlin, D.B., 1924, *ApJ*, **60**, 22

[Mullen & MacDonald 2001] Mullen, D.J. and MacDonald, J., 2001, *ApJ*, **559**, 353-371

[Perryman et al. 1997] Perryman, M.A.C. et al., 1997, *A&A*, **323**, L49-L52

[Pickering 1880] Pickering, E.C., 1880, *Proc.Am.Acad.ArtsSci*,, **16**, 257

[Rossiter 1924] Rossiter, R.A., 1924, *ApJ*, **60**, 15

[Salpeter 1952] Salpeter, E.E., 1952, *PR*, **88**, 547-553

[Thomas & Weiss 1992] Thomas, J.H. and Weiss, N.O., 1992, Sunspots: Theory and Observations, *NATOASISeries*, *C375Dordrecht* : *Kluwer*.

[Thomas & Weiss 2008] Thomas, J.H. and Weiss, N.O., 2008, Sunspots and Starspots, *Cambridge*: *Cambridge University Press*.

[Valenti & Piskunov 1996] Valenti, J.A., and Piskunov, N., 1996, *A&AS*, **118**, 595

[Vogt 1981] Vogt, S.S., 1981, *Astrophys.J.*, **247**, 975

[Vogt & Penrod 1983] Vogt, S.S. and Penrod, G.D., 1983, *Pub.Astron.Soc.Pacific*, **95**, 565

[Winn et al. 2010] Winn, J.N. et al., 2010, *ApJL*, **723**, L223-L227

[Yi et al. 2001] Yi, S.K., et al. 2001, *ApJS*, **136**, 417